applied sciences

MDPI

Review

Molten Salt Mixtures as an Energy Carrier for Thermochemical Processes of Renewable Gas Production: Review and Perspectives

Marco D'Auria [1], Anna Chiara Tizzoni [1], Francesco Rovense [1,*], Salvatore Sau [1], Luca Turchetti [1], Diogo Canavarro [2], João Marchã [2], Pedro Horta [2] and Michela Lanchi [1]

[1] ENEA—Italian National Agency for New Technologies, Energy and Sustainable Economic Development, Via Anguillarese, 301, 00123 Rome, Italy; marco.dauria@enea.it (M.D.); annachiara.tizzoni@enea.it (A.C.T.); salvatore.sau@enea.it (S.S.); luca.turchetti@enea.it (L.T.); michela.lanchi@enea.it (M.L.)

[2] University of Évora–Renewable Energies Chair, Polo da Mitra da Universidade de Évora, Edifício Ário Lobo de Azevedo, Nossa Senhora da Tourega, 7000-083 Évora, Portugal; diogocvr@uevora.pt (D.C.); joaomarcha@uevora.pt (J.M.); phorta@uevora.pt (P.H.)

* Correspondence: francesco.rovense@enea.it

Abstract: This study provides a comprehensive review of molten salt technology, as well as electrochemical and thermochemical processes aimed at hydrogen and syngas production. First, this research illustrates the current types of molten salt mixtures, detailing their main applications and thermophysical properties. Then, the analysis delves into existing thermo-electrochemical cycles and their specific operating conditions for producing hydrogen and syngas. Moreover, this study assesses the compatibility of these processes with molten salt integration. This investigation involved a comprehensive review of the existing technical and scientific literature, blending insights and practical experiences to offer detailed data on the topics explored. The findings suggest that molten salts, with their medium–high operating temperatures, can markedly improve the efficiency and sustainability of hydrogen and syngas production. Furthermore, this study outlines the pivotal role these technologies can play in achieving the European Union's ambitious goals by enhancing the use of renewable energy sources and advancing the shift to carbon-free solutions.

Keywords: thermo-electrochemical processes; molten salt mixture; renewable syngas production; hydrogen production

check for updates

Academic Editor: Raffaele Marotta

Received: 18 April 2025
Revised: 6 June 2025
Accepted: 17 June 2025
Published: 19 June 2025

Citation: D'Auria, M.; Tizzoni, A.C.; Rovense, F.; Sau, S.; Turchetti, L.; Canavarro, D.; Marchã, J.; Horta, P.; Lanchi, M. Molten Salt Mixtures as an Energy Carrier for Thermochemical Processes of Renewable Gas Production: Review and Perspectives. *Appl. Sci.* **2025**, *15*, 6916. https://doi.org/10.3390/app15126916

Copyright: © 2025 by the authors. Licensee MDPI, Basel, Switzerland. This article is an open access article distributed under the terms and conditions of the Creative Commons Attribution (CC BY) license (https://creativecommons.org/licenses/by/4.0/).

1. Introduction

Climate change is causing increasingly severe impacts globally, requiring immediate and effective responses. The European Union (EU) has proactively addressed these challenges through several strategic initiatives. The European Green Deal, launched in 2019, aims to achieve climate neutrality by 2050 and foster sustainable economic growth, resource efficiency, innovation, and social inclusivity [1]. Key policies such as the "Fit for 55" legislation support this vision, targeting a fair and economically viable reduction in greenhouse gas emissions by at least 55% by 2030, relative to 1990 levels [2]. All 27 EU Member States have committed to these ambitious climate goals, making Europe the first continent aiming for climate neutrality.

In 2021, the EU Commission launched "Next Generation EU", a major funding program to support economic recovery and accelerate Europe's green and digital transition [3]. Subsequently, the REPowerEU plan was introduced to boost renewable energy deployment, increase energy efficiency, diversify energy sources, and reduce dependence on fossil

fuels [4]. In March 2023, the EU strengthened its commitment by raising the binding target for renewable energy to at least 42.5% by 2030, with an aspirational goal of 45%.

To further advance its strategy, the EU Commission adopted a dedicated solar energy plan in May 2022, aiming for more than 320 GW of solar capacity by 2025 and nearly 600 GW by 2030. This was supported by revised regulations, including the updated Renewable Energy Directive, to streamline permitting and accelerate the deployment of renewable energy projects [5]. Advanced solar technologies, such as Concentrated Solar Power (CSP), are central to the EU's renewable energy strategy. By integrating thermal energy storage (TES), these systems enable on-demand electricity generation and help address the intermittency of solar resources. However, for CSP to play a significant role in the EU energy mix, further progress is needed to improve cost competitiveness through both technological innovation and economies of scale. Meanwhile, energy storage is becoming increasingly essential for stabilizing fluctuations in electricity supply and demand.

As energy systems increasingly rely on renewable energy sources (RESs), energy storage has become ever more crucial in achieving a carbon-neutral economy. Hydrogen, in particular, is emerging as a key element in this transition and features prominently in several EU policies. Both the European Green Deal and REPowerEU emphasize the instrumental role of renewable hydrogen in supporting secure, affordable, and sustainable energy solutions, including the development of hydrogen valleys. Furthermore, under the Net-Zero Industry Act of the Green Deal, hydrogen fuel cells are identified as critical technologies. The Green Deal's Act also ensures the availability of important materials for electrolyzers and RES, supporting the secure and clean production of renewable hydrogen. At the international level, the Clean Hydrogen Mission of Mission Innovation aims to reduce the cost of renewable hydrogen and promote the development of hydrogen valleys worldwide. These coordinated efforts are strengthening the integration of hydrogen in Europe, enabling the supply of renewable energy to households, industries, and the transport sector.

Acting as an energy carrier, hydrogen has the capability to transport and store vast amounts of energy derived from renewable sources over extended periods, or directly serve as a fuel, particularly within industrial and transport applications [6]. This positions it as a key component in the clean energy transition. The increasing importance of renewable, often termed "green" or "clean", hydrogen is critical for Europe to meet its climate change objectives, reduce greenhouse gas emissions, and achieve strategic energy independence through domestic production [7]. Moreover, years of dedicated research and innovation have placed the EU at the forefront of global hydrogen technology, spanning the entire value chain from production to storage, distribution, and a multitude of final uses across all economic sectors [8]. Therefore, the EU's focus on renewable hydrogen—produced via electrolysis powered by renewable sources—has positioned it at the forefront of global hydrogen technology, covering the entire value chain from production to end-use applications [9].

Molten salts (MSs), known for their high thermal stability and heat transfer ability, can effectively store thermal energy from renewable sources, such as CSP. This capability facilitates the wholly renewable production of hydrogen, as well as other fuels, by harnessing solar energy efficiently. Moreover, MSs can store excess renewable energy generation, allowing for the decoupling of solar energy collection from the production of renewable gases, using that energy on-demand to drive thermochemical reactions for gas production outside of sunlight hours.

Therefore, the exploration of MS technology for the supply of thermal energy to thermochemical processes presents a novel and potentially transformative approach for the

production of renewable hydrogen and syngas, promising to align with the EU's strategic initiatives to advance clean energy technologies and reduce greenhouse gas emissions.

The primary aim of this work is to provide a comprehensive overview of three critical areas: (1) the use of MS mixtures as heat transfer fluids and storage media, including their feasible operational conditions and thermophysical properties; (2) hydrogen production processes; and (3) syngas production processes that can be integrated with MS technology. This research was conducted as part of a Joint Research Activity in the SALTOpower project, which aims to advance excellence in research by further exploiting MS technologies. The research activities specifically focus on the development of a flexible interconnection between power and gas energy distribution systems, aiming to facilitate the generation of power and/or gas using medium-to-high-temperature renewable heat sources. The insights derived from this study are intended to contribute significantly to the development of scalable and sustainable energy systems to align with the EU's long-term goals for energy security and environmental sustainability. Regarding the methodology adopted for the collection of contributions, priority was given to articles providing data useful for the practical application of molten salts. Drawing on the consolidated experience of the authors on the topics addressed, both related publications produced by the authors themselves and those considered most significant with respect to the subjects discussed were included. In cases where the topic did not fall within the direct experience of the authors, the selection of articles to be cited was carried out mainly using the Scopus platform, giving preference to contributions most relevant to the applications considered. This manuscript is organized as follows: in Section 2, the main applications for MSs are outlined, along with the most used types and their thermophysical properties. Additionally, the advantages and disadvantages of using MSs both as heat transfer fluid and as a storage medium are discussed. Section 3 details the three main types of thermo-electrochemical cycles used for hydrogen production, showcasing the system configurations and operational conditions. Section 4 provides a comprehensive description of the various layouts and processes involved in the production of syngas, detailing the specific conditions under which these processes are conducted. Section 5 presents brief assessments of the feasibility of MS-driven processes for gas production, with a focus on heat supply considerations. Finally, Section 6 presents the conclusions, further work, and future research directions.

2. Molten Salt Mixtures

Thanks to their unique combination of properties, such as high thermal stability, good heat transfer capabilities, and wide operational temperature ranges, MSs are being considered for application across a spectrum of industrial and energy applications. In the chemical industry, they catalyze a variety of processes, enabling high-temperature reactions that are otherwise challenging to manage. Within nuclear reactors, MSs have been studied as coolant systems and as the medium for nuclear fuel in advanced reactor designs, promising safer and more efficient energy production. Their use extends significantly to RES, where they are now employed both as a heat transfer fluid and as a storage medium. Notably, in CSP plants, they facilitate electricity generation even when solar irradiance is absent. Beyond energy production, molten salts offer innovative solutions in waste treatment processes, where their chemical properties enable the detoxification, recovery, and recycling of valuable materials from industrial residues [10].

The choice of salt type hinges on an understanding of the chemical and thermodynamic properties required by the different applications. Salts must exhibit high chemical and radiolytic stability at elevated temperatures, favorable freezing and boiling points, a significant specific heat capacity, and thermal conductivity and must maintain low vapor pressure to ensure operational integrity [11].

Thermal exchange and storage materials are fundamental components of a CSP plant, affecting both the efficiency and the costs of the generated electric power [12]. Currently, MSs are the most used materials in CSP for temperatures above 100 °C as a heat storage medium (HSM) and a heat transfer fluid (HTF). They are attractive candidates, having high heat capacity, high density, high thermal stability, relatively low costs, no flammability, and very low vapor pressure, which leads to a storage design without pressurized vessels [12]. In general, MSs are defined as ionic liquids and classified according to anions and cations. In practice, the minimum operating temperature is mainly defined by liquidus temperature, that is, the solidification onset. Clearly, it is necessary to avoid freezing inside the piping, the heat exchanger, and the storage tanks. For this reason, an auxiliary back-up heating system is required in an MS-CSP plant.

Nitrate/nitrite mixtures are studied and developed for the low and medium temperature of Parabolic Trough Collector (PTC) CSP. Chloride salts and their mixtures are particularly relevant as working fluids for high temperature (>400 °C) applications in solar power tower plants [13]. CSP with other anhydrous oxyanion salts (e.g., carbonates) and halide salts (e.g., fluorides and chlorides) is currently strongly limited: it is present only in theoretical studies and thermal analysis measurements, not in real commercial applications [14]. Indeed, its main shortcomings are a relatively very high freezing point presented by the salts and their mixtures and compatibility with containment materials, the latter problem being especially relevant for molten carbonates. However, a few molten mixtures of inorganic salts are presented in the literature as thermal energy storage (TES) for high temperatures, such as sodium hydroxide, which operates at a temperature between 320 °C and 800 °C.

2.1. Molten Salt Mixtures as Heat Transfer Fluid and Storage Medium

MSs are predominantly utilized for the storage of heat, presenting a sustainable method for capturing and storing thermal energy. Their main application is found in CSP plants and nuclear facilities [15], where their capacity to store vast amounts of heat at elevated temperatures facilitates the generation of electricity and/or heat. Nitrates and nitrites are among the most commonly used HTFs in current applications. However, the production of these salts is geographically and quantitatively limited, with the majority of global reserves located in Chile and Peru [15].

In nuclear facilities, an instance of application is Nuclear Energy Systems (NESs), comprising two primary components: an MS loop that transfers heat through a secondary coolant from the nuclear reactor to a storage tank, and a power cycle loop, which includes various power cycles converging at the point of common coupling. These cycles might use Rankine, Brayton, or combined Air–Brayton configurations, utilizing different working fluids to generate power. A variant of an NES is its hybrid version, which combines various energy generation systems to enhance efficiency. This includes incorporating nuclear reactors, renewable energy sources, process heat applications, and different energy storage solutions [16].

Regarding CSPs, they transfer thermal energy by collecting solar radiation using an array of mirrors or heliostats to concentrate it onto a receiver, which then transfers the heat, directly or indirectly, to the MS. Technologies such as PTC, solar power towers, and linear Fresnel reflectors are instrumental in this process. Each varies in its method of concentrating solar energy but is unified in its objective to maximize the capture of thermal energy and its transfer to the MS.

A prime example of MS use in CSP systems is “solar salt”, a binary mixture of 60% $NaNO_3$ and 40% KNO_3 by weight. Its ability to remain thermally stable in a liquid state at temperatures of up to 600 °C enables efficient heat transfer and energy storage,

exemplified in the Solar Two central receiver system in California and numerous solar thermal plants in Spain [17]. The first demonstrations in Europe of MS deployment in linear CSP configurations include projects like the experimental facility PCS of the ENEA Casaccia Research Centre (Italy) and the direct MS loop located at Priolo Gargallo (Sicily, Italy), addressing the integration challenges in CSP technology [18]. For the storage of MSs, sophisticated containment systems are employed, designed to minimize heat loss and ensure the longevity and safety of the stored thermal energy. These systems typically involve insulated storage tanks that can maintain the high temperatures of MSs without significant thermal degradation over time. The storage tanks are engineered from materials specifically chosen for their resistance to the corrosive properties of MSs and their ability to endure thermal stresses arising from temperature fluctuations [15].

There are two primary types of MS thermal storage options utilized in CSP plants: the thermocline system and the two-tank system. The two-tank system operates on a principle where a hot tank and a cold tank separately store the salt, akin to conventional storage schemes in CSP plants. Conversely, the thermocline system employs a single tank that houses both cold and hot salt layers. In a thermocline tank, the salt layers are divided by a thermocline—a sharply defined layer where the temperature changes dramatically. This layer acts as a barrier, preventing the hot and cold salts from mixing, thereby maintaining distinct thermal zones within a single storage vessel. When charging, the cold salt moves from the tank's colder region, passes through a heat exchanger, and enters the warmer section, effectively storing thermal energy. During discharge, the process reverses, with the hot salt flowing out through the heat exchanger back to the colder part of the tank. A significant challenge in MS thermal energy storage systems is the risk of the salt freezing, given its high melting point. To mitigate these issues, several strategies are essential to maintain the salt in a liquid state and ensure its effective circulation. First, thermal insulation of storage tanks and piping is crucial to retain heat within the system. Additionally, auxiliary heating systems can prevent the MS from freezing by activating when the temperature approaches its melting point. Continuous circulation of the MS prevents solidification by maintaining uniform heat distribution. Active temperature control systems that monitor and adjust the MS temperature can prevent temperatures from falling below the freezing point. Drainage systems are also beneficial; they allow for the salt to be drained from receivers and pipes during downtime, storing it in thermally insulated tanks to prevent freezing. Pre-heating the system before start-up after a period of inactivity is necessary to ensure the salt returns to a liquid state. Implementing thermal tracing on piping using heating cables or tapes can maintain the salt's temperature above its melting point. Operational strategies, such as pre-heating the system during colder hours or maintaining minimum temperature overnight, are employed to prevent freezing. These measures, individually or in combination, play a key role in the operational reliability and efficiency of CSP systems, addressing the challenges associated with MS thermal management [15].

2.2. Molten Salt Mixtures' Thermophysical Properties

The use of nitrate mixtures both as an HTF and as a sensible HSM, and less frequently as a Phase Change Material (PCM) [19], has been investigated since the 1980's [20,21], with a particular focus on solar salt. This composition presents several favorable characteristics, including upper temperature limits (around 600 °C), lower unit costs, better safety aspects, and low environmental impacts [22]. Although this nitrate mixture does not represent a eutectic composition, its higher proportion of sodium nitrate is preferable, as this significantly reduces material costs while avoiding an increase in the liquidus temperature. However, its practical operating temperature range is limited by two key factors: an initial solidification temperature

of approximately 240 °C and an upper operational limit of about 590–600 °C [23,24]. Currently, no methods have been proposed to effectively increase the upper temperature stability limit of molten salt nitrates, aside from short-term effects [25] that are not useful for a CSP plant where the maximum temperature is to be maintained over long periods of time. Moreover, experimental results show that the use of cations different from those of first group metals leads to a decrease in nitrate chemical stability [26,27].

For the reasons mentioned above, recent research has focused on reducing the initial solidification temperature of nitrate mixtures. Lowering this temperature could decrease the costs associated with thermal insulation and backup heating systems in CSP plant pipelines and could also simplify start-up and maintenance procedures.

To address the drawback of solar salt's relatively high freezing temperature, MS mixtures with significantly lower melting temperatures (<150 °C) have been proposed in the scientific literature.

In general, the addition of other cations, such as lithium and calcium, and different anions, such as nitrites (e.g., $NaNO_2$), has been explored. Conversely, the use of metal cations, such as silver, cesium, and rubidium [28,29], has been considered unrealistic, with mixtures containing $AgNO_3$, $TlNO_3$, and $RbNO_3$ studied only from an academic perspective [29,30]. The ternary nitrate mixture $Na/K/Ca//NO_3$ (commercially known as Hitec XL®) offers practically the same safety advantages as solar salt, combined with favorable thermophysical properties and a reduced freezing temperature of approximately 120 °C. However, it exhibits lower thermal stability compared to solar salt [26,27]. Due to its relatively low costs, comparable to solar salt, this mixture is suitable for use both as an HTF and as an HSM in active, direct storage systems. Another attractive option involves lithium-containing mixtures. However, given lithium's comparatively higher costs, these mixtures have been considered economically viable only as an HTF (with solar salt serving as the HSM) within indirect storage systems employing an intermediate heat exchanger between the two fluids [14]. Literature findings indicate that the economic advantage achieved by reducing costs related to thermal insulation and backup heating systems is completely offset by the expenses incurred for an intermediate heat exchanger. Therefore, no significant economic benefit is observed. Ternary $Li/K/Ca//NO_3$ additive systems have also been investigated; however, these mixtures exhibit no appreciable improvement over the $Na/K/Ca//NO_3$ system and are likely to be more expensive due to the substitution of sodium with lithium. Mixtures containing nitrites, such as the Hitec® fluids, exhibit initial solidification temperatures and chemical stability similar to ternary systems, like Hitec XL®, although they are more expensive and exhibit higher toxicity. Additionally, quaternary mixtures, such as $Ca/Li/Na/K//NO_3$, show freezing points and anticipated costs only marginally lower than those of lithium-containing ternary mixtures. However, the presence of calcium tends to lower their maximum operating temperature [26], resulting in reduced efficiency of the thermoelectric power conversion process. Additionally, quaternary and quinary reciprocal mixtures (such as $Li/Na/K//NO_2/NO_3$ and $Ca/Li/Na/K//NO_2/NO_3$, respectively) have been proposed [31], yet their increased complexity does not correspond to a meaningful improvement in thermophysical properties. Recently, novel senary mixtures have been investigated, showing considerably lower melting temperatures, reaching values as low as 56 °C.

Molten chloride salts can be used as an HTF and as an HSM for both sensible [32] and latent heat storage [33]. Other metal halides, such as fluorides and bromides, are expectably more expensive, and the former present particularly severe issues regarding corrosion [34].

Fluoride salts and container materials for TES applications are in the temperature range of 973 to 1400 K [35]. On the other hand, their freezing point is generally higher

than that for molten nitrates [36], and they can be extremely corrosive and require costly containment materials [37–39].

Among the several possible formulations, chlorides of the first and second group are of particular interest, given their relatively low costs and high availability. For instance, the Na/K/Mg//Cl eutectic (with a molar percentage of around 47/23/30 for $MgCl_2$/KCl/NaCl, respectively) presents a quite advantageous price, below 0.35 USD/kg, and a melting point of 385 °C [40]. Villada et al. [40] reported an acceptable volatility below 800 °C, density and thermal conductivity comparable (but at higher temperatures) to solar salt, and a dynamic viscosity ranging from about 2 cP (at 800 °C) to around 5 cP near the freezing temperature. A problem using this mixture derives from the high hygroscopicity of $MgCl_2$, which leads to corrosion issues and also affects salt stability in the presence of air [41]. Similar considerations can be made for the Na/K/Ca//Cl additive eutectic (51.7/7.5/40.8 mol% for $CaCl_2$/KCl/NaCl, respectively), with a price estimated as half of that of solar salt and a melting point of 497 °C [42].

Several mixtures of the Na/K/Zn//Cl system were evaluated by NREL [43]. They exhibit a significantly high density (up to 2.4 g/mL) and acceptable price (0.8 USD/kg), but present high volatility, especially above 700 °C.

Molten carbonates can be potentially employed at higher temperatures than nitrates, but costly cations are to be used in order to obtain mixtures with an acceptable freezing point.

The Na/K/Li//CO3 ternary eutectic has a melting temperature of 398 °C and an estimated cost of 2.5 USD/kg, and it was proposed to be used as an HTF at up to 650–700 °C [43,44]. This temperature increase might increase the overall solar-to-electric conversion efficiency by 18.5% more with respect to systems operating at 565 °C with molten nitrates [45]. In addition to molten chlorides, molten carbonates present substantial issues regarding material compatibility, also depending on the gas atmosphere [39]. Mixed anion (reciprocal) mixtures have mainly been proposed for TES as a PCM [46,47]. However, the solubility of carbonates and chlorides in molten nitrates is limited [21]: a recent scientific paper reports a sizable increase regarding chemical stability (i.e., the maximum operating temperature), if chlorides are added to nitrate mixtures [48].

Table 1 lists the names of the main MS mixtures; the type of mixture; and thermophysical properties, such as the mean value of density ($\overline{\rho}$) and specific heat ($\overline{c_p}$) in the operating temperatures, the melting temperature (T_{melt}), and the decomposition temperature (T_{deco}); and the references from which these properties were derived.

Table 1. Molten salt mixtures: composition and thermophysical properties.

Mixture [-]	Type of Mixture [-]	Composition [%wt.]	T_{melt} [°C]	T_{deco} [°C]	$\overline{\rho}$ [kg m^{-3}]	$\overline{c_p}$ [J kg^{-1} °C^{-1}]	Refs.
Nitrate-based							
Solar salt	Binary	60 $NaNO_3$ 40 KNO_3	240	565	1834	1512	[24,49]
Hitec®	Ternary	7 $NaNO_3$ 53 KNO_3 40 $NaNO_2$	142	450	1721	1560	[28,50,51]
Hitec XL®	Ternary	15 $NaNO_3$ 43 KNO_3 42 Ca $(NO_3)_2$	130	450	2000	1449	[27,52,53]

Table 1. *Cont.*

Mixture [-]	Type of Mixture [-]	Composition [%wt.]	T_{melt} [°C]	T_{deco} [°C]	$\bar{\rho}$ [kg m^{-3}]	$\bar{c_p}$ [J kg^{-1} °C^{-1}]	Refs.
			Nitrate-based				
LiNaK//NO_3	Ternary	30 $LiNO_3$ 18 $NaNO_3$ 52 KNO_3	118	550	1884	1580	[54–56]
LiNaKCa/NO_3	Quaternary	15.5 $LiNO_3$ 8.2 $NaNO_3$ 54.3 KNO_3 22 Ca $(NO_3)_2$	93	450	1803	1518	[57–59]
$LiNaKNO_3NO_2$	Quaternary	9 $LiNO_3$ 42.3 $NaNO_3$ 33.6 KNO_3 15.1 KNO_2	97	450	1877	1155	[60]
			Chloride-based				
KMgCl	Binary	62.5 KCl 37.5 $MgCl_2$	430	>700	1857	999	[61–63]
NaKMgCl	Ternary	20.5 NaCl 30.9 KCl 48.6 $MgCl_2$	383	>700	1669	1024	[35,61]
NaMgCaCl	Ternary	39.6 NaCl 39 $MgCl_2$ 21.4 $CaCl_2$	407	650	2557	1104	[64–66]
NaKZnCl	Ternary	7.5 NaCl 23.9 KCl 68.6 $ZnCl_2$	204	>700	2207	901	[62,66,67]
KMgZnCl	Ternary	49.4 KCl 15.5 $MgCl_2$ 35.1 $ZnCl_2$	356	>700	1857	866	[61,62,66]
			Fluoride-based				
LiNaKF	Ternary	29.2 LiF 11.7 NaF 59.1 KF	454	>700	2109	1590	[68,69]
NaBF	Binary	3 NaF 97 $NaBF_4$	385	>700	1866	1506	[51]
KBF	Binary	13 KF 87 KBF_4	460	>700	1792	1305	[70]
KZrF	Binary	32.5 KF 67.5 ZrF_4	420	>700	2680	1000	[51]
			Carbonate-based				
$LiNaKCO_3$	Ternary	32.1 Li_2CO_3 33.4 Na_2CO_3 34.5 K_2CO_3	397	670	2038	1610	[71]

To offer a comparative assessment of their thermophysical properties, the authors selected and studied four commonly employed molten nitrate/nitrite mixtures, among the ones mostly employed as an HTF and an HSM for CSP applications [22,72]. Table 2 lists the thermophysical properties of the MS mixtures considered here for the comparison. The solar salt properties can be compared with those of three alternative MS mixtures.

Table 2. Thermophysical properties of solar salt, Hitec®, Hitec XL®, and lithium-containing ternary MS mixtures [72].

Property	Value	Unit
Solar Salt		
Chemical composition	$NaNO_3/KNO_3$ (60/40)	%wt.
Density	$\rho = 2090 - 0.63 \cdot T$	kg m^{-3}
Dynamic viscosity	$\mu = 71{,}645 \cdot T^{-1.763}$	Pa s
Thermal conductivity (max. operation temperature)	$k = 0.3804 + 3.452 \cdot 10^{-4} \cdot T$	W m^{-1} K^{-1}
Heat capacity	$c_p = 1.5404 + 3.0924 \cdot 10^{-5} \cdot T$	kJ K^{-1} kg^{-1}
Thermal stability	600	°C
Liquidus temperature	238	°C
Hitec® (Na/K nitrate/nitrite)		
Chemical composition	$NaNO_3/KNO_3/NaNO_2$ (7/53/40)	%wt.
Density	$\rho = -0.9 \cdot T + 2269.4$	kg m^{-3}
Dynamic viscosity	$\mu = 146{,}452 \cdot T^{-1.903}$	Pa s
Thermal conductivity	$k = 0.5843 \mp 0.0006 \cdot T$	W m^{-1} K^{-1}
Heat capacity	$c_p = 1.55 - 0.0001 \cdot T$	kJ K^{-1} kg^{-1}
Thermal stability (max. operation temperature)	450 under air; 530 under inert gas	°C
Liquidus temperature (initial solidification point)	141	°C
Hitec XL® (Na/K/Ca nitrate)		
Chemical composition	$NaNO_3/KNO_3/Ca(NO_3)_2$ (15/43/42)	%wt.
Density	$\rho = 2240 - 0.827 \cdot T$	kg m^{-3}
Dynamic viscosity	$\mu = 509{,}611 \cdot T^{-2.072}$	Pa s
Thermal conductivity	$k \cong 0.519$ (Constant in the operating range)	W m^{-1} K^{-1}
Heat capacity	$c_p = 1.542 - 0.000322 \cdot T$	kJ K^{-1} kg^{-1}
Thermal stability (max. operation temperature)	≤425	°C
Liquidus temperature (initial solidification point)	~125	°C
Na/K/Linitrate		
Chemical composition	$NaNO_3/KNO_3/LiNO_3$ (18/45/37)	%wt.
Density	$\rho = 2051 - 0.6639 \cdot T$	kg m^{-3}
Dynamic viscosity	$\mu = 58{,}725 \cdot T^{-1.69}$	Pa s
Thermal conductivity	$k = 0.0005 \cdot T + 0.4$	W m^{-1} K^{-1}
Heat capacity	$c_p = 1.5395 + 0.0003 \cdot T$	kJ K^{-1} kg^{-1}
Thermal stability (max. operation temperature)	600	°C
Liquidus temperature (initial solidification point)	120	°C

Regarding the temperature working limit for these materials, a proper criterium may be to avoid the detectable production of nitrogen or NOx. According to the scientific literature, this reaction can occur through several mechanisms [14,21,73,74], but the result is invariably the formation of metal oxides, followed by hydroxide and carbonate production, if the mixture is in contact with moisture and carbon dioxide [22]. If nitrites are present, they are oxidized into nitrates above a certain temperature threshold. It is interesting to note that alkaline nitrates undergo an equilibrium reaction with oxygen which becomes relevant above 550 °C [14,75–77]:

$$MNO_3 \rightleftharpoons MNO_2 + ½\ O_2 \qquad (M = Na, K, Li) \tag{1}$$

In general, a limited presence of nitrite is not considered a cause of chemical degradation, given its low impact on the mixture's thermophysical properties [22].

In this context, Table 2 reports the temperature limits under air atmosphere, unless where differently specified. Regarding the solar salt mixture, Steinbrecher et al. [78,79] reported a significant increase in its chemical stability, up to 650 °C, using, as the cover

gas, nitrogen containing oxygen and small amounts (ppms) of NO, while the presence of nitrogen instead of air led to limited effects.

Figure 1 shows a comparison between the thermophysical properties of the HTFs considered within their respective operating temperature ranges, referring to operations in ambient air (except where specified differently); however, they can be extended beyond these limits by operating in a controlled atmosphere [72].

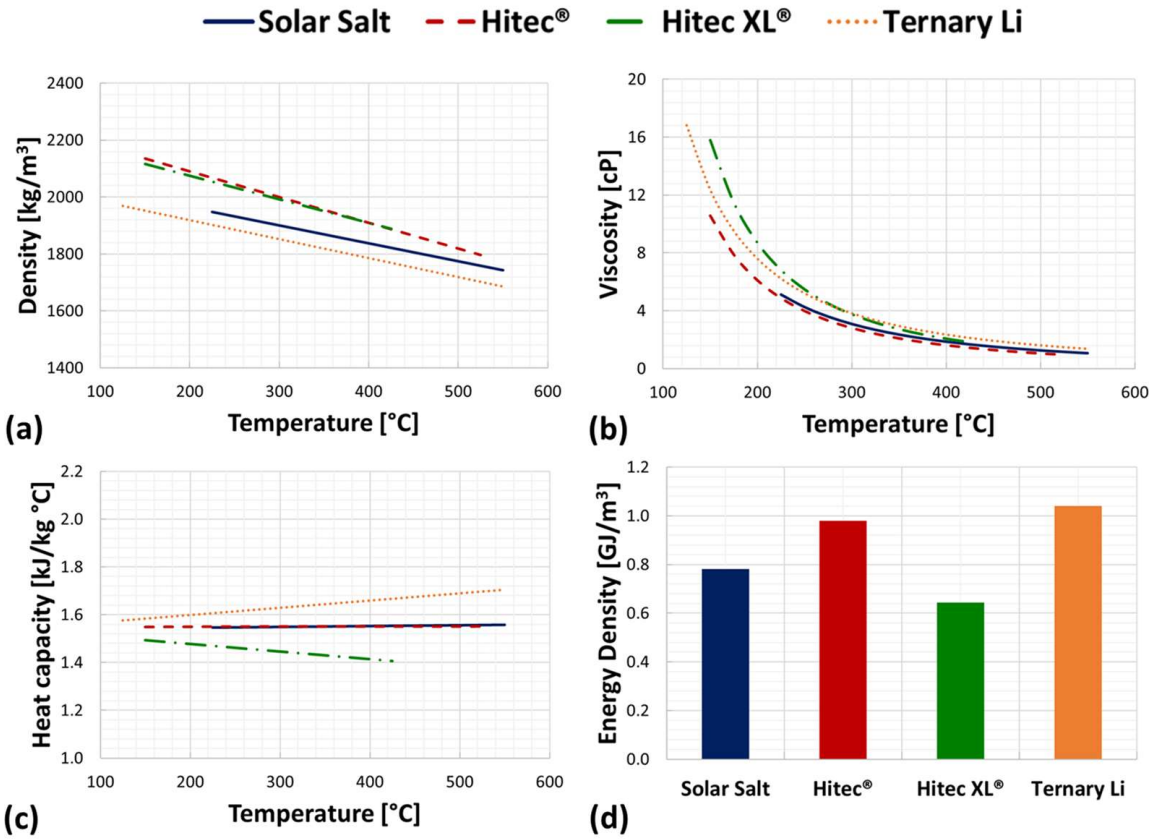

Figure 1. Comparison between the densities (**a**), the dynamic viscosities (**b**), the heat capacities (**c**), and the volumetric energy densities (**d**) of the four salts in the following respective operation ranges: 290–550 °C for solar salt; 200–530 °C for Hitec®; 200–425 °C for Hitec XL®; and 200–550 °C for Na/K/Li nitrate [72].

Moreover, the volumetric densities were estimated, considering sensible heat release and average values for densities and heat capacities in the respective operation ranges: 290–550 °C for solar salt; 200–530 °C for Hitec®; 200–425 °C for Hitec XL®; and 200–550 °C for Na/K/Li nitrate.

Besides thermophysical properties, an assessment of different HTF solutions includes the assessment of corrosion issues related to the steel components of a CSP plant, such as pipes, valves, tanks, welding joints, etc. Specifically, molten nitrates show some drawbacks linked to the degradation of nitrates into nitrites, with possible oxygen generation, when the fluid is heated 295 °C [80].

Studies carried out so far on steel corrosion with mixtures of molten nitrates are not adequately systematic. Furthermore, these tests sometimes provide contradictory results; there are no validated/shared methods for carrying out corrosion tests.

From the results available in the open literature, it can be concluded that less expensive carbon steels may be employed for mixtures operating at low temperatures (200–400 °C), while for higher temperatures (400–600 °C), special stainless steels or alloys containing nickel, which have a higher corrosion resistance, should be considered [81].

Toxicity and environmental compatibility are clearly major issues for large-scale utilization of heat transfer materials. MSs are safe and in general not toxic. However, nitrites and lithium can also be harmful for humans and the environment, and the thermal decomposition of nitrates and nitrites can lead to the formation of nitrogen oxides [22].

From the comparison proposed in this document, it is possible to assess the following [72]: (1) the commercial MS mixture Hitec® is characterized by the presence of sodium nitrite and shows a relatively low freezing point, together with good features concerning specific heat, density, and viscosity. However, this material is toxic and less thermally stable than solar salt under air [22]; (2) an interesting alternative is represented by the MS mixture composed of calcium, potassium, and sodium nitrates, Hitec XL® [73]. However, its viscosity is much higher than that of solar salt, especially at temperatures approaching the freezing point, while its thermal stability in the presence of air is similar to that of Hitec® [22].

The addition of lithium nitrate significantly decreases the freezing point of an MS mixture, while, at the same time, similar thermophysical properties and stability of solar salt can be obtained [22]. However, the costs and availability of lithium can represent an issue for its utilization in CSP plants with a large-scale TES capacity.

3. Thermo(-Electro-)Chemical Processes for the Production of Hydrogen and Syngas

For several decades, the use of hydrogen as an energy carrier, and not only as a raw material in the process industry, has been considered as a potential key element in facilitating the transition process towards the decarbonization of energy systems. This interest is motivated by the fact that the combustion of hydrogen is not associated with the production of carbon dioxide, and the same gas can be used in fuel cells to produce electrochemical electricity, with much higher efficiencies than thermal combustion.

Currently, most hydrogen is used in industrial processes and is produced from fossils, with an associated huge amount of CO_2 emissions (about 8 tons per 1 ton of obtained hydrogen) [82]. These emissions are due both to the chemical reactions that characterize the hydrogen formation process and to the combustion of carbonaceous sources, which is necessary to thermally support the process. For the use of hydrogen as an energy vector to be fully sustainable, carbon dioxide emissions must be reduced, and the integration of renewable sources into production processes is a fundamental requirement to achieve this. In particular, the use of solar energy is one of the main options currently being considered.

Figure 2 shows a diagram of the main processes for producing hydrogen and syngas using water and/or a carbon source (fossil or biological) as the primary source and can be operated with high-temperature heat and/or electricity, depending on the type of process considered.

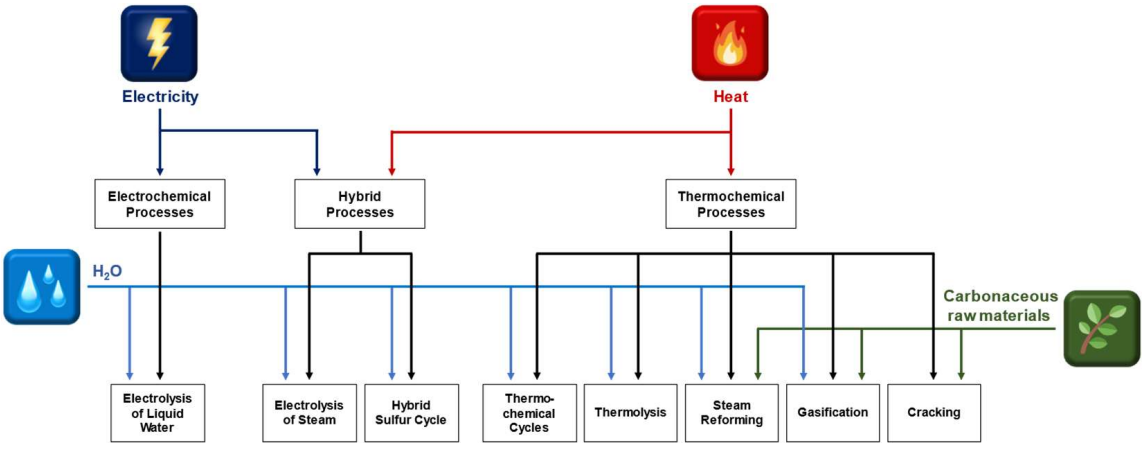

Figure 2. Processes for hydrogen and syngas production.

There are two main approaches for hydrogen production, depending on the primary source used. On the one hand, conventional production processes based on the transformation of carbonaceous feedstocks (e.g., steam reforming of natural gas) with RESs are used to thermally support the process. Unless the carbon source is of renewable origin (e.g., biogas or biomethane) and a CO_2 capture system is provided, this approach does not completely solve the emissions problem, but it does, however, allow for important environmental sustainability benefits. First, emissions are significantly reduced by replacing fossil fuels with RES. Furthermore, by carrying out fuel decarbonization at the centralized level where it is easier to achieve CO_2 capture, distributed emissions at the level of individual utilities are avoided. Another key aspect is related to the possibility of using processes widely established in the chemical industry which are suitable for large-scale production. In this way, the use of RESs in industrial hydrogen production can be encouraged with the aim of a more radical process transformation. The second approach focuses on producing hydrogen exclusively from water using RES, resulting in a completely carbon-free fuel.

Hydrogen production processes can be classified into three main categories based on the type of energy used: (1) The first is thermochemical processes, which require thermal energy typically in the range of 500 to 1000 °C. Conventional methods like steam reforming and gasification of carbonaceous feedstocks fall under this category. Another promising thermal route is Water Splitting Thermochemical Cycles (WSTCs), which have been developed since the 1970s and offer significant potential. (2) The second is electrochemical processes, which primarily use electrical energy. An example is the electrolysis of liquid water, a well-established industrial process, although currently not widely deployed at a large scale. Alkaline electrolysis and Proton Exchange Membrane (PEM) cells are the most commercially viable options, often coupled directly or indirectly with photovoltaic (PV) systems. (3) The third is hybrid processes, which utilize a combination of both electrical power and heat. They are often integrated with PV and CSP systems. Examples include hybrid WSTC cycles and high-temperature electrolysis using Solid Oxide Electrolysis Cells (SOECs), which offer potential efficiencies superior to alkaline or PEM processes.

4. Steam Electrolysis and Thermo(-Electro-)Chemical Cycles

Nowadays, the most widespread technology is water electrolysis, preferably integrated in an RES production grid. Currently, the electrolysis plants installed in the EU account for 24 MW from solar sources and 500 MW from wind energy. Regarding further developments of this methodology, some problems are still present, and, in particular, it would be necessary to reduce investment costs and increase the electrolyzer's lifetime [83]. Another issue is the resistance under numerous start and stop cycles.

Regarding the other routes, pilot plants up to a TRL of 5–6 have been developed for thermochemical and hybrid water splitting cycles and also for steam reforming [84]. Almost always, the RES is from CSP, and, in this respect, the integration with high-temperature storage systems represents a major challenge.

Regarding water electrolysis, production costs can be evaluated at about 5–6 EUR/kg for plants connected to an electric grid, with a target of 1–3 EUR/kg [85]. Off-grid productions instead present significantly higher costs of around 8–10 EUR/kg.

Regarding thermochemical cycles, the absence of industrial-scale plants means that production costs are estimated through techno-economic analyses. FCH-JU reported 10 EUR/kg in 2017, with the target of reaching 8 and 6 EUR/kg for, respectively, 2020 and 2023 [86]. Similar values are also expected for high-temperature electrolysis.

Steam reforming coupled with CSP presents the most promise in terms of cost efficiency. In fact, from data obtained with a pilot plant, it was possible to establish costs below 4 EUR/kg for hydrogen and electric-power co-production [87].

4.1. High-Temperature Electrolysis

In high-temperature electrolysis (HTE), water is heated by an external heat source, entering the electrolytic cell in the form of steam, to promote the decomposition of the water molecule (see Figure 3).

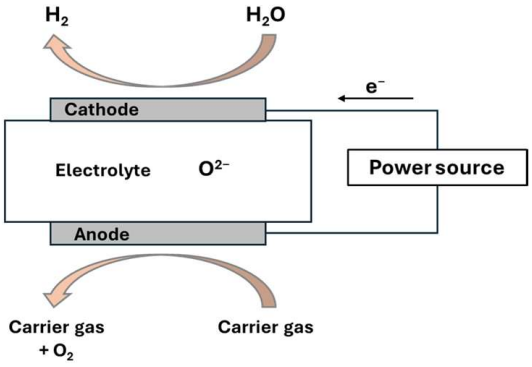

Figure 3. Schematic representation of HTE process, adapted from Ref. [87].

One possible heat source is CSP: the high radiative fluxes allow for operations at desired temperatures (600–800 °C). Figure 4 shows a schematic representation of a possible P&ID of the process.

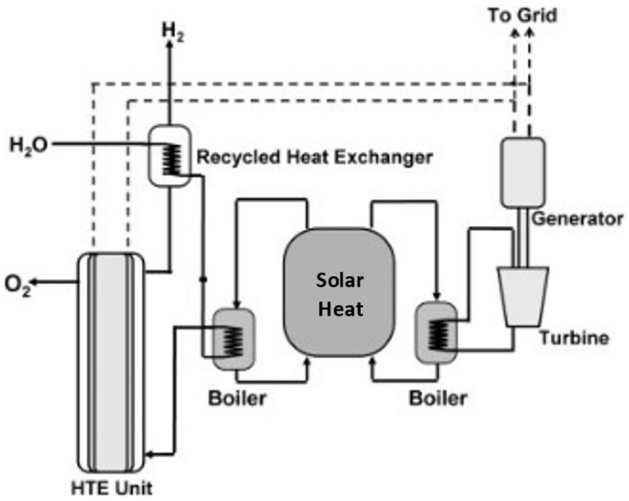

Figure 4. Schematic P&ID of a CSP-HTE process, adapted from Ref. [87].

Considering hydrogen production efficiency as a performance indicator, defined as the ratio between the higher heating value of hydrogen and the sum of the gross electrical energy plus the thermal energy required to produce the hydrogen, it is possible to achieve values of approximately 52.6% at 0.4 MPa and 800 °C [87]. More recently, some companies with "Sunfire" reported conversion values of 84% in practical tests (PCI H_2 to AC) [88].

HTE requires both thermal and electrical energy to decompose steam into hydrogen and oxygen. In the electrolysis reaction, the electrical energy input is equivalent to the Gibbs free energy change (ΔG), while the thermal energy input corresponds to TΔS (where T is the reaction temperature, and ΔS is the entropy change). As the reaction temperature rises, the required electrical energy ΔG decreases, while the necessary thermal energy TΔS increases (Figure 5). Consequently, high-temperature electrolysis demands less electrical energy input compared to electrolysis conducted at lower temperatures. In comparison with conventional electrolysis, HTE can present the following benefits: (1) It requires lower working voltages (<1 V vs. standard 1.23 V) due to the energy contribution of the thermal component (ΔH = ΔG + TΔS) (Figure 5). (2) It allows for the combination with feedstock

(e.g., biomass) at high temperatures to react with oxygen ions. In practice, part of this energy from this feedstock is used to "assist" the electrolysis process and thus reduce hydrogen production costs [89].

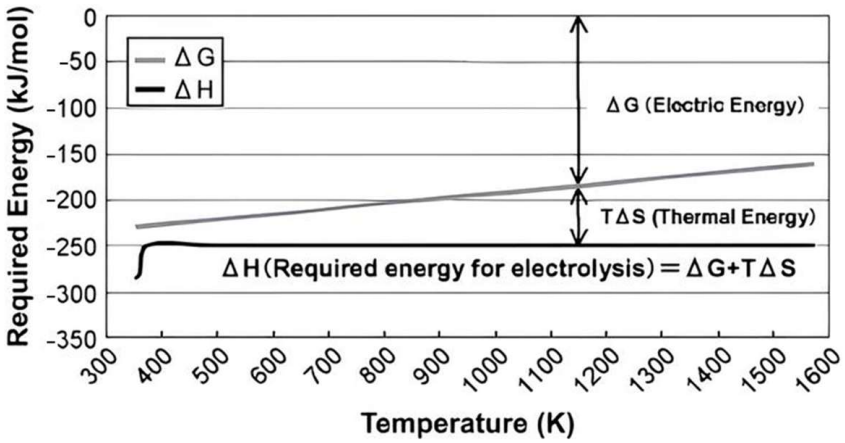

Figure 5. In the HTE process, the ΔH value has a contribution from TΔS, hence reducing the working voltages necessary when compared to conventional electrolysis (from Ref. [87]).

4.2. Water Splitting Thermochemical Cycles

WSTCs are multi-step processes where chemical intermediates are cyclically consumed and regenerated, water is the only inlet species, and hydrogen and oxygen are the only products [90].

Each of the cycle steps occurs at a different temperature, with a maximum level between 800 °C and 1500 °C. Processes with a maximum temperature below 1000 °C are of particular interest, given their feasibility to be coupled with CSP and IV generation nuclear reactors, like high-temperature gas reactors.

The research on WSTCs focuses on processes compatible with the temperatures available from CSP plants and MS mixtures. ENEA was directly involved in the investigation of three thermochemical cycles (see Table 3), developing both lab-scale experimental facilities and simulation models. The sulfur–iodine and the modified sulfur–iodine processes were studied in the national project FISR-TEPSI (Tecnologie e Processi innovativi per affrontare la transizione e preparare il futuro del Sistema Idrogeno) and in the EU project HyCycles (materials and components for hydrogen production by sulfur based thermochemical cycles) [91–93], while ferrites were considered within INNOHYP (innovative high-temperature routes for hydrogen production) Project.

Table 3. Main characteristics of thermochemical cycles for hydrogen production.

Process	No. of Steps	Reactions	Pros (+) & Cons (−)	Ref.
Sulfur–iodine	3	$2H_2O + I_2 + SO_2 \rightarrow H_2SO_4 + 2HI$ **(Bunsen reaction, 20–120 °C)** $2HI \rightarrow I_2 + H_2$ **(300–500 °C)** $H_2SO_4 \rightarrow H_2O + SO_2 + 1/2\ O_2$ **(800–1000 °C)**	+ Liquid or gaseous intermediates (easily manageable in chemical plants) + Use of commonly available chemical species − Complex and numerous separation steps − High corrosive intermediates − Presence of iodide and iodide-based compounds − The second and third reaction generally requires catalysts	[91,92]

Table 3. *Cont.*

Process	No. of Steps	Reactions	Pros (+) & Cons (−)	Ref.
Modified sulfur–iodine (NIS)	5	$2H_2O + I_2 + SO_2 \rightarrow H_2SO_4 + 2HI$ **(Bunsen reaction, 20–120 °C)** $Ni + H_2SO_4 \rightarrow NiSO_4 + H_2$ **(20–100 °C)** $NiSO_4 \rightarrow NiO + SO_2 + ½\ O_2$ **(≈900 °C)** $NiO + 2HI \rightarrow NiI_2 + H_2O$ **(≈100 °C)** $NiI_2 \rightarrow Ni + I_2$ **(≈600 °C)**	+ Less corrosive intermediates + All reactions with high rates, near to 100%, without the necessity of catalysts + Possibility to easily store, if necessary, intermediate compounds − Numerous separation steps − Toxic compounds, if Nickel is used	[93]
Mixed ferrites	2	$2MnFe_2O_4\ (s) + 3Na_2CO_3\ (s) + H_2O \rightarrow 6Na(Mn_{1/3}Fe_{2/3})\ O_2\ (s) + 3CO_2\ (g) + H_2\ (g)$ $6Na(Mn_{1/3}Fe_{2/3})O_2\ (s) + 3CO_2\ (g) \rightarrow 2MnFe_2O_4\ (s) + 3Na_2CO_3\ (s) + 0.5O_2$	+ In principle, only gas–solid reactions, with easy separation processes + Reaction temperature below 800 °C, if ferrite nanoparticles (2–20 nm) are used − Costly material preparation − Need to operate with excess water in the first step, leading to high-energy-consuming operations for recovering pure hydrogen (unless proper separation membranes are developed)	[94]

The sulfur–iodine cycle has the advantage of being based on liquid or gaseous intermediates, which are readily transportable in a chemical reaction plant. The major drawbacks are complex separative processes and issues regarding corrosion. In particular, the Bunsen reaction needs to be performed with a large excess of iodine in order to separate sulfuric acid and hydriodic acid (HI) solutions; the former is still purified and concentrated by heating [95], and the latter undergoes another separation process (typically, an energetically expensive distillation [96]) to remove iodine from HI. In the most common schemes, sulfuric acid results at a concentration of around 80 wt.% [91], while hydriodic acid is obtained at the azeotropic composition (57 wt.%) [91]. Both acids are then thermally decomposed [97–99], and in both cases, a heterogeneous catalyst is needed in order to operate with acceptable temperatures and reaction rates. Another problem is represented by the limited thermodynamic conversion for HI cracking [91].

Some of the concerns presented by the sulfur–iodine process may be overcome by employing oxides, sulfates, and iodides as intermediates (modified sulfur iodine) [93,100]. This alternative route was validated using nickel compounds, as described in Table 3. Hydrogen is quantitively produced, reacting to metallic nickel with sulfuric acid, avoiding the necessity of catalysis. The obtained sulfate is decomposed at around 900 °C into nickel oxide, sulfur dioxide (to be reused in the Busen section), and oxygen. Then, it is necessary to retrieve metallic nickel, and this can be achieved by forming nickel iodide (from NiO plus HI) and decomposing that salt into iodine (recycled into the Bunsen reactor) and elemental nickel. Overall, there are clear advantages regarding the thermodynamic yield of each phase, the use of acids only at low temperatures (improving corrosion issues), the absence of catalysts, and the possibility of storing intermediate products also for long times. On the other hand, the number of steps is increased, and nickel compounds are quite toxic.

A totally different approach is exemplified by the mixed-ferrite cycle. In the example reported in Table 3, both steps can be carried out below 800 °C [94,101]. While in routes like sulfur–iodine or similar commonly available chemicals, in these processes, nanostructured mixed oxides are appositely synthesized. As a result, only gas solid reactions are present,

thus simplifying the necessary equipment and the separation processes. The disadvantages are the high preparation costs of ferrites and the necessity, in the first step, to operate with a large excess of steam with respect to the stoichiometry; this leads to the problem of separating the produced hydrogen from a substantial amount of water and, unless a proper separation membrane will be developed, to a drastic decrease in the global cycle efficiency.

4.3. Hybrid Thermochemical Cycles

In hybrid thermochemical cycles, water is split into hydrogen and oxygen using different types of energy sources, such as solar, electricity, biomass combustion, and so on.

Likely, the most investigated hybrid method is the so-called Westinghouse cycle, which is a simplification of sulfur–iodine, where nothing changes regarding oxygen production, while hydrogen is formed by electrolysis of a SO_2 aqueous solution—SO_2 Depolarized Electrolysis (SDE)—where sulfuric acid is produced at the anode and hydrogen at the cathode. With respect to direct water electrolysis, the oxidation of aqueous sulfur dioxide is thermodynamically more favorable than O_2 oxidation, and, actually, the SDE process can be carried out, saving 40 to 75% of electric power with respect to alkaline H_2O electrolysis [102,103]. In this context, ENEA was a partner in the SOL2HY2 (Solar-To-Hydrogen Hybrid Cycles) EU project, where it was mainly involved in developing a proper catalyst to be used in a solar reactor present at the DLR Centre of Jülich [104]. An important aspect of this project was to study the feasibility of using SO_2 from industrial wastes to feed the cycle in periods with insufficient solar irradiation. In this regard, ENEA developed simulation tools to investigate the coupling of the process with TES systems based on molten nitrates and the possibility to use a contemporary central receiver system and a PTC plant in order to ensure the continuity of hydrogen production.

Another, and a very peculiar, alternative hybrid route is represented by the sulfur–ammonia cycle, where the disproportionation of the ammonium sulfite intermediate, thermodynamically spontaneous under reaction conditions, is catalyzed with the energy of light photons and the presence of photocatalytic materials. ENEA participated in the validation of this cycle, in particular, regarding the thermal part of the process, in the framework of the national funding scheme PRIN2019 [105]. Both processes are summarized in Table 4.

Table 4. Main characteristics of hybrid thermochemical cycles for hydrogen production.

Process	No. of Steps [1]	Reactions [2]	Pros (+) & Cons (−)	Ref.
Westinghose process	2	$SO_2 + 2H_2O \rightarrow H_2SO_4 + H_2$ **(elettrochemical, T < 100 °C)** $H_2SO_4 \rightarrow H_2O + SO_2 + ½\ O_2$ **(T ≈ 850 °C)**	+ No iodide and iodide compounds are present + Easier separation procedures than the "sulfur–iodine" process − Issues regarding the efficiency of the electrolysis step	[102,103]
Sulphur–ammonia cycle	3 + 1 (SO_2, NH_3 absorption in water)	$(NH_4)_2SO_3 + H_2O \rightarrow (NH_4)_2SO_4 + H_2$ **(photocatalytic, T < 100 °C)** $(NH_4)_2SO_4 \rightarrow 2\ NH_3 + H_2O + SO_3$ **(T ≈ 400–500 °C)** $SO_3 \rightarrow SO_2 + ½\ O_2$ **(T ≈ 850 °C)** $SO_2 + H_2O + 2NH_3 \rightarrow (NH_4)_2SO_3$ **(T < 100 °C)**	+ No iodide and iodide compounds are present + No necessity for electric power − Photocatalytic hydrogen production is quite slow	[105,106]

[1] Excluding separation steps. [2] In all cases, summing up all steps, water splitting is obtained: $H_2O \rightarrow H_2 + ½\ O_2$.

5. Thermochemical Conversion of Carbonaceous Feedstocks

5.1. Steam Reforming

The methane steam reforming process is the most widely used industrial process for producing hydrogen [107]. It is a chemical process commonly carried out at temperatures above 850 °C in furnaces fired by fossil fuels.

Methane steam reforming essentially consists of two gas-phase catalytic reactions between steam and methane:

$$CH_4 + H_2O \rightarrow CO + 3\,H_2,\ \Delta H\ (298\ K) = +206\ kJ/mol \quad (2)$$

$$CO + H_2O \rightarrow CO_2 + H_2,\ \Delta H\ (298\ K) = -41\ kJ/mol \quad (3)$$

Reaction (1) of steam reforming of de-sulfurized natural gas is strongly endothermic and is usually carried out at 800–1000 °C in furnaces fired with raw natural gas. In contrast, Reaction (2), which maximizes the hydrogen yield, and is known as the Water–Gas shift reaction, is exothermic and hence favored at lower temperatures (200–450 °C). The hydrogen produced is subsequently separated from the gas mixture by pressure swing adsorption, while CO_2 can be captured by adsorption in aqueous amino–alkali solutions. A process diagram of methane steam reforming is shown in Figure 6.

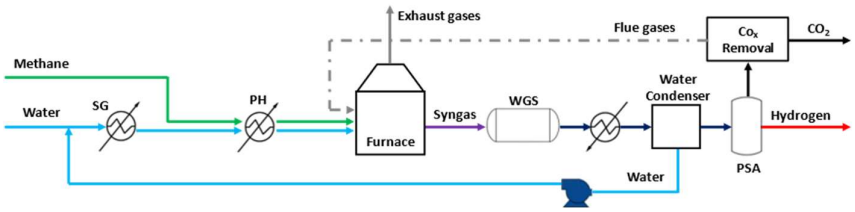

Figure 6. Schematic diagram of the methane steam reforming process, adapted from Ref. [108].

5.2. Gasification

Biomass gasification represents a way to increase the use of biomass for energy production, permitting widespread use of biomass [109–111]. It consists of the conversion of solid/liquid organic compounds, in which partial oxidation of the carbon in the feedstock occurs, leading to the formation of a gas/vapor phase and a solid phase: The gas phase, otherwise called synthesis gas or syngas, can be used for power generation or can be upgraded for biofuel production. The solid phase (char) includes unconverted organic fraction and ash. During the gasification process, the carbonaceous biomass is converted into syngas, a mixture consisting mainly of H_2, carbon monoxide (CO), CO_2, and methane (CH_4). This is generally carried out in the presence of a suitable gasifying agent or oxidants, such as air, oxygen, steam, or carbon dioxide.

In this process, four main steps can be distinguished:

- Oxidation (exothermic);
- Drying (endothermic);
- Pyrolysis (endothermic);
- Reduction (endothermic).

The classification of gasification is based on several parameters, such as the types of gasifiers, gasification temperature, heating (direct or indirect), and gasifying agent. According to the biomass, gasification technology, and operating conditions [112–115], the Lowest Heating Value (LHV) of syngas can vary from 4 to 13 MJ/Nm^3, while the LHV of char can range from 25 to 30 MJ/kg.

Gasification reactors are classified into three main categories [116]: cross-flow reactors (>50 MW_{th}), fluidized-bed reactors (5–100 MW_{th}), and fixed-bed reactors (100–10,000 kW_{th}). The former requires a very high temperature (2000 °C [116]), pure oxygen, and steam as a gasifying agent in addition to high-quality fuels, so this category does not seem to be the best solution for coupling with MS technologies. Regarding fluidized-bed reactors, which are certainly effective when high exchange coefficients are required and where the fluidization fluid coincides with the heat transfer fluid, the associated technological difficulties and high costs make it convenient for CSP to apply this solution only to large plants (>100 MW_{th}). In addition, since fluidized-bed reactors have an operating temperature of 700–800 °C throughout the reactor, it would not be feasible to combine them with a commercial CSP plant, which can only supply heat up to a maximum temperature of 550 °C (using MS as the HTF). Fixed-bed reactors, on the other hand, work at temperatures between 800–1400 °C, with low reaction rates, and are the most common (78%) [116].

Briefly, reactors in this category can be classified into three types, differentiated by the modes of gas phase efflux: up-draft, cross-draft, and down-draft.

The up-draft reactor (1–10 MW_{th}) is the simplest type and has a maximum flow rate of about 4 t/h, with strict grain-size requirements (see Figure 7). Biomass enters from the top, while the gasification agent inlet is at the base of the reactor. Above the inlet, the gasification agent finds the grid where biomass that has already released volatiles is oxidized. In this zone, it is possible to exceed 1000 °C. This phase promotes both the formation of ash, which precipitates through the grate and is collected at the bottom, and the production of hot gases. Moving upward, heat is transferred to the zone where the reduction process takes place. Further up, the hot gases meet the pyrolysis zone, where volatile components are released, and then the drying zone, where the biomass is dehydrated. At this point, the gases exit at 200–300 °C. This type of reactor has high thermal efficiency, but a syngas with a high tar content is obtained, because pyrolysis occurs in the part of the reactor where the volume is not large enough to guarantee contact times at high and adequate temperatures to ensure the reduction and thermal cracking reactions, also due to the lowering of the temperature due to the evaporation of the water in the biomass.

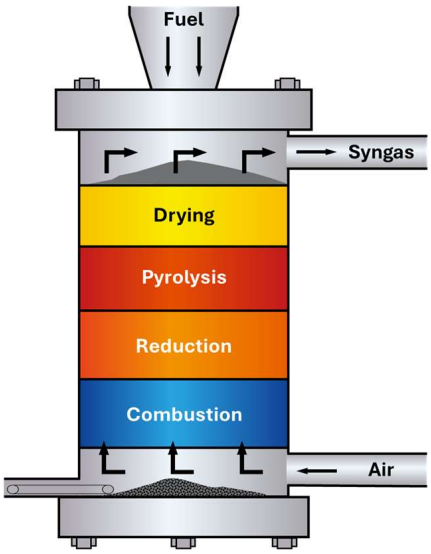

Figure 7. Diagram of up-draft reactor, adapted from [117].

In a cross-draft reactor (Figure 8), the air flow crosses the biomass, which is fed from the top of the reactor and exits from the bottom. In the zone where air is injected as the oxidizing agent, some oxidation and reduction reactions occur due to the high temperatures reached. Heat received in the proximity passes (mainly by conduction) to the pyrolysis and drying zones, concentric to the central zone, where very high temperatures can be reached (1500 °C [118]), while at the gas outlet, the temperature is about 800–900 °C [116]. Tar production is very low (0.01–0.1 g/Nm^3), and ash is collected at the bottom of the reactor. The technical difficulties and small size of this type of reactor, combined with the lower conversion efficiency, limit its widespread use.

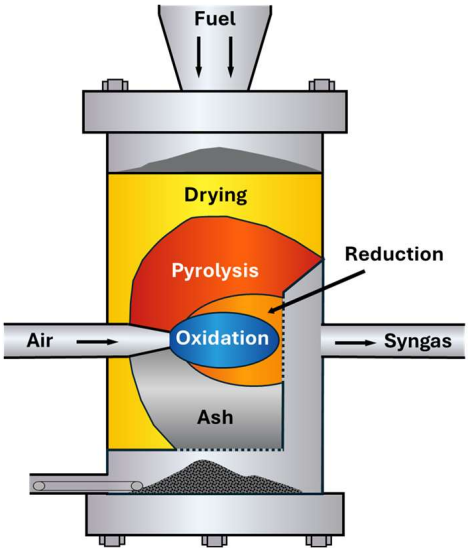

Figure 8. Diagram of cross-draft reactor, adapted from [119].

The down-draft reactor (Figure 9) is the one most used, especially for its small size, from a few tens to a few hundred thermal kW. In this case, the gaseous stream, consisting of water and the vapors produced by the drying and initial thermal degradation processes of biomass, coming from the top of the reactor flows down in the same direction as the solid fuel. The output in the pyrolysis zone, with its high tar content, passes through the zone where part of the fuel is burned and where a temperature of 1200–1400 °C is reached [118]. This area is where thermal cracking occurs and where the chemical reactions of many reactants begin, which also take place in the lower part of the reactor. In fact, char, gaseous hydrocarbons, and tars react with steam at high temperatures with endothermic reactions to give CO and H_2, processes also favored by the presence of alkaline-earth compounds that catalyze reforming reactions. As a result of these thermochemical processes, the tar content present in the syngas can vary in the range of 0.015–3.0 g/Nm^3, in contrast to the 30–150 g/Nm^3 obtained in up-draft reactors. On the other hand, the amount of particulate in the syngas at the outlet is much higher than in the other configurations. This is because the gas, as it leaves the reactor through the bottom, passes through the support grid along with ash and dust, which remain suspended in the gaseous stream. The gas stream, which is heated by the oxidation zone, in this case, does not pass through the drying and pyrolysis zones, which results in lower thermal efficiency (in addition to the need to use biomass with a low moisture content). In this configuration, the drying, pyrolysis, and gasification zones are well separated, so the gas does not heat the pyrolysis reactions, which can be powered by solar energy up to a temperature of 500 °C. This aspect will be important for matching the solar system under consideration.

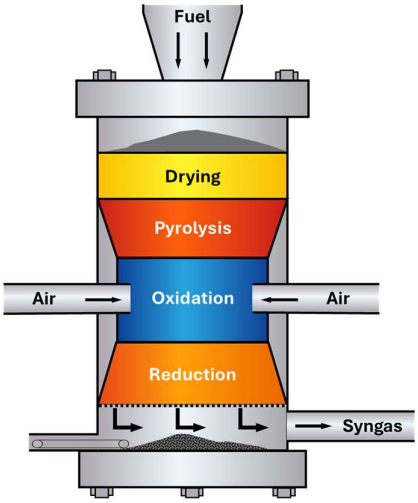

Figure 9. Diagram of down-draft reactor, adapted from [120].

5.3. Hydrothermal Gasification

Unlike reforming and dry gasification, hydrothermal gasification is a biomass conversion process where relatively lower temperatures (around 600 °C versus 800–1200 °C) and significantly higher pressures (above 25 MPa) are used [121–123]. Water is used as the reaction medium, and this technology is suitable for wet biomasses and organic wastes, avoiding the costly drying step of feedstocks.

Hydrothermal gasification processes can be classified, according to the reaction temperatures, into the following: (1) The first is aqueous phase reforming, with temperatures ranging from 215 °C to 265 °C. If the feedstock concentration is very low (about 1%), it is thermodynamically possible to obtain hydrogen. The main output products are H_2 and CO_2. Subcritical conditions are not suitable for gasifying high-molecular-weight constituents, like lignin or cellulose [124–126]. (2) The second is near critical gasification, with temperatures ranging from 350 °C to 400 °C. Biomass is gasified at near critical gasification conditions to obtain high degrees of carbon conversion to methane [127]. (3) The third is supercritical water gasification (SCWG), with a temperature higher than 374 °C (usually higher than 500 °C) to obtain H_2 and CO_2 as the main products. This process shows high conversion rates; however, it is highly dependable on factors like operation conditions, feedstocks, the nature of the catalyst (if used), or the reactor design. In this type of gasification, supercritical water has a twofold role as a reactant and medium of biomass. Under supercritical conditions, an optimal environment is created for hydrolysis and pyrolysis reactions due to the generation of H+ and OH− ions [126]. In addition, free radicals are generated, enhancing gas formation, leading to a high gas yield [127]. Because of the higher solubility and reactivity of organic compounds in supercritical water, SCWG produces less tar and char as a by-product, in comparison with conventional dry gasification. This has dual benefits: tar and char are difficult to gasify; on the other hand, they cause a reduction in the energy efficiency of the process by means of reactor plugging, heat exchanger fouling, and catalyst deactivation [128].

5.4. Pyrolysis

Pyrolysis is a thermochemical process that transforms material such as wood, agroforestry, or plastic waste into gaseous, liquid, and solid compounds, without the presence of oxygen. Depending on the operating conditions, the pyrolysis process can occur at temperatures between 200 °C and 1000 °C and at pressures of up to 100 bar.

Outputs vary with process and feedstock conditions. In general, it can be said that there are three main outputs [129]:

- Biochar (10–30%);
- Bio-oil (20–50%);
- Syngas (20–30%).

The pyrolysis process can occur under three major operating conditions: slow pyrolysis, intermediate pyrolysis, and fast/flash pyrolysis [130]. Table 5 presents a summary of the features of each operating condition.

Table 5. Operating conditions for pyrolysis processes.

Operating Condition	Operating Temperature	Residence Time	Main Output	Compatibility with Use of MS
Slow pyrolysis	200–400 °C	5–30 min	Biochar	Yes, if above 290 °C
Intermediate pyrolysis	400–600 °C	1–5 min	Bio-oil	Yes, if up to 565 °C
Fast/flash pyrolysis	600–1000 °C	1–2 s	Syngas	No

CSP technologies can be coupled to such processes, as through their concentration factor, such operating temperatures can be achieved and, eventually, can increase the Lower Heating Value of the produced syngas by a factor of 1.4–1.9 [131].

Operating costs are relatively difficult to identify in the literature, as they depend on the intended output and operating conditions. However, it is possible to state costs between EUR 75–300 per ton of oil (12–54 EUR/MWh), assuming a feedstock cost between 0–100 EUR/t (0–1.9 EUR/GJ) [129].

On the other hand, a recent NREL study for a 550-metric-ton/day dry wood fast/flash pyrolysis plant producing 106 million liters of bio-oil per year concluded that the capital cost is 46 M EUR and the operating cost will be 9.1 M EUR/year (based on a product value of 0.16 EUR/l) [132].

It is also important to note that the pyrolysis process can be combined with other thermochemical processes, as shown in Figure 10 [133]. The advantage of such combinations is to diversify and/or increase the efficiency of biomass waste conversion in multiple outputs, such as hydrogen, fuels, heat power, etc.

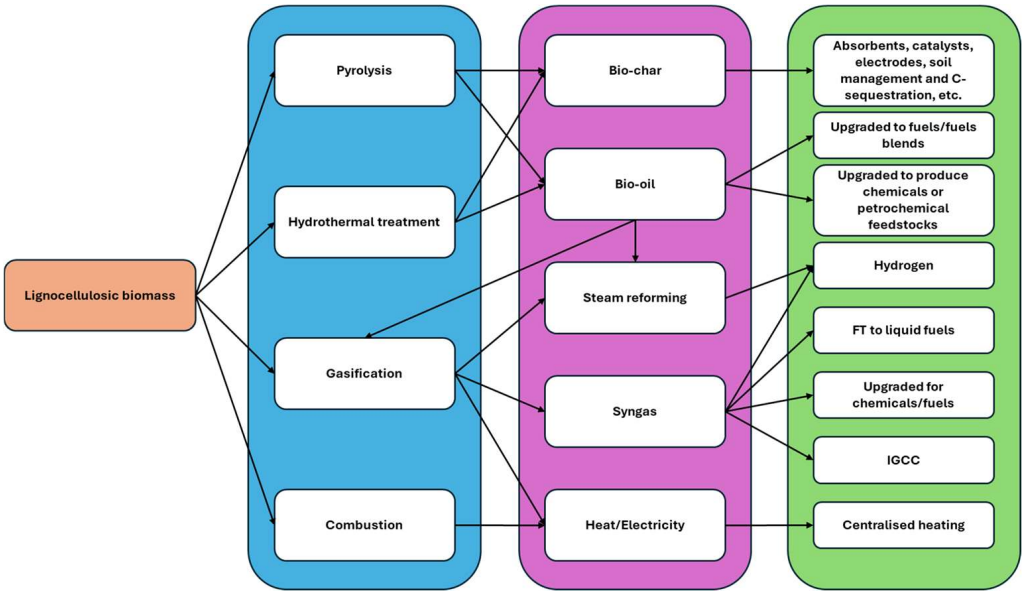

Figure 10. Pyrolysis process can be combined with other thermochemical processes for the production of multiple outputs. Here, a flow-chart of a possible thermochemical conversion process for lignocellulosic biomass is presented, adapted from [133].

Regarding methane-containing mixtures (e.g., natural gas, biogas, and biomethane), pyrolysis methodologies can be considered as ways to produce hydrogen with zero CO_2 emissions, without the need to use systems for carbon dioxide capture [134]. Actually, these processes allow for straightforward coupling with an HTF and the TES used in CSP and can lead to a direct separation of carbon and H_2, where the former can be stored in a solid state and, if valuable products are obtained, placed on the market. This way, the usual "carbon sequestration" route can be replaced by "carbon valorization" methods [135,136].

Among the different possible approaches, a very innovative and interesting one is to perform the pyrolysis reaction directly in a molten bath made of liquid metals or MSs (typically chlorides) [137]. This is so to avoid the employment and possible poisoning of catalysts, and the carbonaceous products can be readily recovered from above the surface of the melt [138].

In this context, the C-zero consortium realized a TRL 6 plant utilizing the $KCl/MnCl_2$ mixture at 1000 °C and 1 bar, obtaining graphite-like carbon as a co-product [139]. Molten metals were instead used at 1120 °C and 1 bar by Ember-TNO, with the formation of carbon black [140].

5.5. Hydrothermal Liquefaction

Hydrothermal liquefaction (HTL) is a thermochemical conversion process that transforms wet biomass into liquid biofuel, known as bio-oil. This process takes place at a high temperature and pressure in the presence of water [141]. Figure 11 shows the operating temperature range of the HTL process.

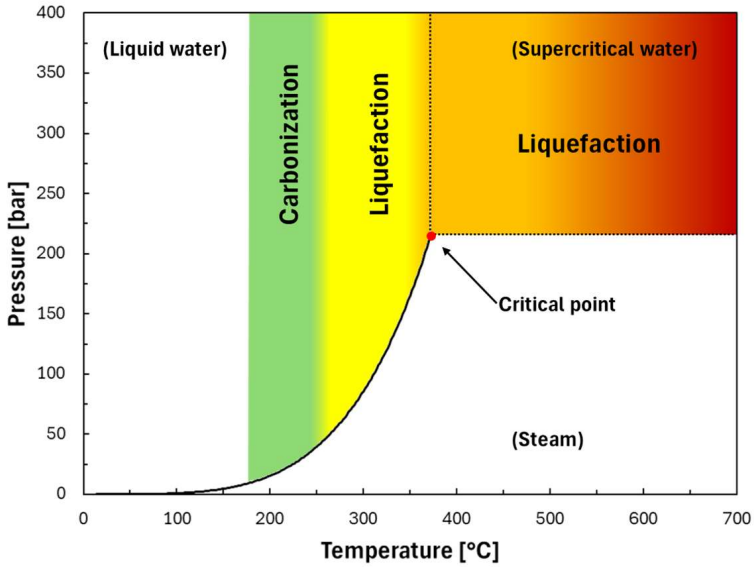

Figure 11. HTL process occurs in a temperature range of 250–400 °C. After the critical point, the process enters a gasification zone where higher gas yields are achieved (adapted from [142] and data from [143]).

Hydrothermal processes may be carried out under a wide range of conditions. At low temperatures (75 °C and 15 bar), a process known as steam explosion occurs, which produces an increment in chemical reactivity and can be seen as a pre-treatment step to separate biomass into its major components for further bioprocessing. As the temperature increases, the macromolecules of the biomass (cellulose and lignin) break up to produce shorter molecules. This leads to hydrothermal carbonization, which occurs at temperatures of 180–250 °C and under pressures of 20–100 bar. However, some fragments polymerize to produce oily substances, which is known as HTL. At pressures of 50 to 200 bar and at temperatures in the range of 200–374 °C, this is the dominant process. Finally, above the

critical point of water, gaseous products like methane, carbon dioxide, and hydrogen predominate in the SCWG process. If the main interest is to produce hydrogen, temperatures and pressures above 600 °C and 300 bar, respectively, are needed.

Due to the high thermal capacity of the biomass–water mixture, hydrothermal processes (HTPs) have higher energy requirements than other transformation processes, like pyrolysis of dry biomass (when the drying heat is not accounted for). Therefore, the possibility of providing this heat through solar energy is very attractive. A few small-scale experimental studies have been carried out with solar reactors for steam explosion, hydrothermal carbonization, HTL, and SCWG. Solar technologies, including PTC, parabolic dishes, and solar furnaces, are utilized to irradiate the high-pressure reactors' walls. However, from the point of view of scalability, theoretical studies have emphasized a different option, indirect heating, where a thermal fluid is first heated in the solar field and then used to heat the reactor. No practical demonstrations of this concept have been reported.

Among the hydrothermal processes described above, HTL and SCWG are well suited to the operation temperature of solar MSs. In fact, CSP technologies can be used as a heat source of this process, but the use of MSs requires a minimum temperature of 290 °C.

Likewise, the cost assessment of the pyrolysis process is not totally clear in the literature. However, it is possible to claim that the minimum fuel selling price of bio-oil is around 2.07 EUR/kg [144].

6. Identification of MS-Driven Processes of Renewable Gas Production

In CSP plants for electricity generation, direct solar irradiance is reflected, concentrated, and converted into high-temperature heat. The thermal energy is then converted to electricity through the use of thermodynamic cycles: in most plants nowadays, solar energy is transferred to an HTF that feeds a steam generator integrated into a Rankine cycle, similar to conventional thermal power plants. The intermediate step of heat generation not only allows for the production of electricity but also feeds heat-demanding processes, for industrial and civil uses, and facilitates schedule electricity generation through technologically mature TES systems, with to the aim of dispatchable generation, which, to date, cannot be pursued through other renewable energy technologies [145]. For this purpose, MS technologies are suitable for use in CSP plants in combination with TES, since MSs can be used both as a heat transfer fluid and as a storage medium.

Although RESs are some of the most interesting and promising solutions for the transition to sustainable energy systems in the future, their main problem is their intermittent nature and fluctuations in their production, which makes it difficult to control and schedule them. Hence, the use of TES increases reliability and facilitates the integration of RESs, allowing for electricity and/or heat release whenever necessary to solve the demand–supply problem and to match peak demands. Therefore, MSs can act as an interface for the constant supply of renewable (high-temperature) heat from multiple sources to industrial processes. In particular, Figure 12 shows a conceptual diagram of the integration of an RES and an MS-TES system to provide heat and power to processes for hydrogen and syngas production, as presented in Section 3.

The following are brief assessments of the feasibility of MS-driven processes for gas production, giving attention to the heat supply. Further details are reported in Tables 6 and 7.

Solid oxide steam electrolysis: Heat is required almost exclusively for this process of steam generation (~1 atm and ~100 °C). The electrolysis process itself is carried out in close-to-adiabatic conditions (thermoneutral potential), and the reactants are pre-heated mostly with heat recovered from the products. Co-electrolysis of H_2O and CO_2 may also be carried out with SOECs, which leads to the production of syngas. Quaternary MS mixtures can be used to supply heat for steam generation.

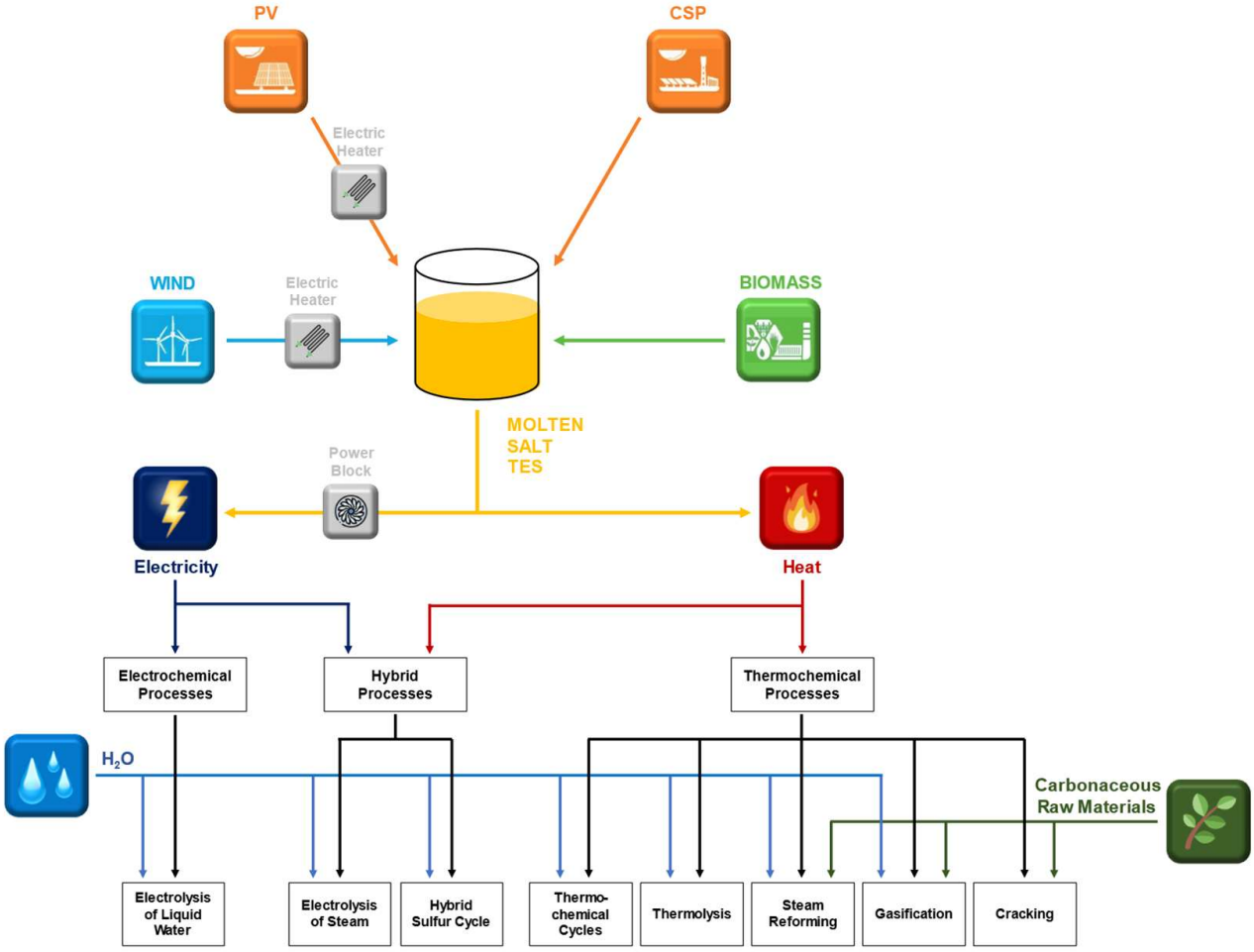

Figure 12. A conceptual diagram of the integration of an RES and an MS-TES system to provide heat and electricity to processes for hydrogen and syngas production.

Molten carbonate steam electrolysis: Heat is required almost exclusively for this process of steam generation (~1 atm and ~100 °C). The electrolysis process itself is carried out in close-to-adiabatic conditions (thermoneutral potential), and the reactants are pre-heated mostly with heat recovered from the products. CO_2 must be fed to the electrolyzer but, overall, is not produced/consumed in the process. CO_2 separation and recirculation may be included to produce H_2 and O_2. Alternatively, outlet H_2/CO_2 mixtures can be fed to other synthetic fuel production processes (e.g., methanol, methane, etc.). Quaternary MS mixtures can be used to supply heat for steam generation.

Sulfur-family cycles: The highest-temperature step of these cycles (SO_3 decomposition) requires heat at 800–900 °C and cannot be served by current commercial MS mixtures. Direct irradiation is currently used to solarize this step. Chloride salts could be considered in the future. Solar salt and other lower-freezing commercial mixtures can be used to supply heat to other process steps, namely, sulfuric acid concentration and SA vaporization and decomposition. Further integration points may be available for specific cycles of this family.

Sulphur–iodine cycle: All information related to sulfur-family cycles can be applied. Furthermore, MSs can be used to supply heat to the hydriodic acid decomposition (endothermic stage at 300–450 °C): 2HI (aq, g) → I_2 (g) + H_2 (g).

Non-volatile metal oxide cycles: Due to the very high temperatures of the high-temperature step, no MS mixtures are available for direct heat supply. Currently, only direct irradiation is considered to supply these processes with solar energy. MSs could be considered for heat recovery/thermal buffering/reactant pre-heating in some parts of the plant.

Mixed ferrites: Some processes, like mixed ferrites, may require CO_2-separation processes, which require heat at ~100–200 °C and could be served with MSs.

Cu-Cl cycle: This is a 4-step hybrid cycle. The highest-temperature thermochemical step is carried out at 530 °C and can be served with solar salt:

$$CuOCuCl_2\ (s) \rightarrow 2\ CuCl\ (molten) + 0.5\ O_2\ (g),\ Thermolysis\ (endothermic) \quad (4)$$

Steam reforming: This conventional high-temperature (700–1000 °C) process is operated by using gas-fired furnaces to produce hydrogen and carbon monoxide, according to the overall reaction.

$$CH_4 + 2\ H_2O \rightarrow CO_2 + 4\ H_2, \quad (5)$$

Consequently, no MS mixture is employable. In order to enable its integration, the steam reforming process can be modified.

Giaconia et al. [146] presented a case study considering a methane steam reformer followed by a water–gas shift section fed with molten nitrates (namely, the solar salt mixture). A methane inlet of 3 kmol/hour is introduced at 20 bars into a tubular reactor, where the molten salt flows counter-currently into an external shell. With a nitrate inlet temperature of 550 °C and an outlet value of 460 °C, a conversion of up to 21% can be obtained for methane into CO_2 and H_2. Very interestingly, as the heat necessary for the endothermic reaction is obtained by the nitrates' sensible heat, which is in turn provided by a parabolic solar trough plant, the produced carbon dioxide drops from 8.3–10.1 $kgCO_2/kgH_2$ (where fossil fuels are employed) to 5.5 $kgCO_2/kgH_2$.

Methane conversion can be still improved by using hydrogen permselective modules, which also makes CO_2 capture easier once separated from H_2 [108,147].

Gasification: In a down-draft reactor, the drying, pyrolysis, and gasification zones are well separated. In this case, the reactions in the pyrolysis step can be powered by MSs up to a temperature of 500 °C.

Supercritical water gasification: In this process, the operating conditions (higher than 374 °C, usually up to 500 °C or above) are compatible with the use of binary solar salt.

Pyrolysis: MS mixtures can be used to supply heat in the slow and intermediate pyrolysis process. Biomass can generically be chemically represented by $C_xH_yO_z$, where the components *x*, *y*, and *z* can be determined by the Total C/H/O (%m/m) divided by the respective MW_C/H/O (g/mol). Slow pyrolysis is characterized by the relatively low operational temperature and longer heating rate values. In intermediate pyrolysis, more C-C connections are broken, and, therefore, there is a tendency to have more bio-oil and syngas.

Hydrothermal liquefaction: In this process, temperatures are moderate (typically 200–400 °C), compatible with the operating temperatures of some MS mixtures.

For electrolysis, after a thorough review of the literature, including studies from previous analyses and based on various works conducted by ENEA, heat is required almost exclusively for this process of steam generation. For the time being, this is not considered a priority, but nevertheless, this process still has some interest, especially when coupled with CSP. In the future, this process will become interesting if electrolyzers that can operate at high pressures are developed: indeed, if electrolysis can be carried out under pressure, the temperature required by this process will be higher, and an MS-driven process can be envisaged.

Table 6. Overview of process parameters and conditions for hydrogen and syngas production.

Process Class	Process Family	Process	Feedstock	Main Products	Process Temperature	Conventional Process Interface	Ref.
Steam electrolysis	Solid oxide steam electrolysis	Solid oxide steam electrolysis	H_2O (+CO_2)	H_2, O_2, and (CO)	600–800 °C	Steam generator (~100 °C)	[148]
Steam electrolysis	Molten carbonate steam electrolysis	Molten carbonate steam electrolysis	H_2O (+CO_2)	H_2, O_2, and (+CO_2)	650 °C	Steam generator (~100 °C) and amine regeneration column reboilers, if CO_2 separation is included	[149,150]
Thermo(-electro-) chemical cycles	Sulfur-family cycles	Sulfur-family cycles	H_2O	H_2 and O_2	Up to >800 °C	Not applicable	[151]
Thermo(-electro-) chemical cycles	Sulfur-family cycles	Hybrid sulfur (Westinghouse) cycle	H_2O	H_2 and O_2	800–900 °C	Not applicable	[102,104,152]
Thermo(-electro-) chemical cycles	Sulfur-family cycles	Sulfur–iodine cycle	H_2O	H_2 and O_2	800–900 °C	Not applicable	[153]
Thermo(-electro-) chemical cycles	Sulfur-family cycles	S-A cycle	H_2O	H_2 and O_2	800–900 °C	Not applicable	[154]
Thermo(-electro-) chemical cycles	Sulfur-family cycles	Modified S-A cycle	H_2O	H_2 and O_2	800–900 °C	Not applicable	[105]
Thermo(-electro-) chemical cycles	Sulfur-family cycles	Modified sulfur–iodine with solid intermediates	H_2O	H_2 and O_2	900 °C	Not applicable	[100,155]
Thermo(-electro-) chemical cycles	Non-volatile metal oxide cycles	Non-volatile metal oxide cycles	H_2O	H_2 and O_2	>1000 °C	Not applicable	[156]
Thermo(-electro-) chemical cycles	Non-volatile metal oxide cycles	Mixed ferrites	H_2O	H_2 and O_2	800 °C	Nost applicable	[157]
Thermo(-electro-) chemical cycles	Metal halide-based hybrid cycles	UT-3	H_2O	H_2 and O_2	760 °C	Not applicable	[158,159]
Thermo(-electro-) chemical cycles	Metal halide-based hybrid cycles	Cu-Cl cycle	H_2O	H_2 and O_2	Up to 500 °C	Not applicable	[160]

Table 6. *Cont.*

Process Class	Process Family	Process	Feedstock	Main Products	Process Temperature	Conventional Process Interface	Ref.
Thermochemical conversion of carbonaceous feedstocks	Steam reforming	Low-temperature steam methane (or biogas) reforming	CH_4, (CO_2), and H_2O	H_2 + syngas	500–550 °C	Not applicable (the conventional high-temperature process is operated at T > 800 °C by using gas-fired furnaces)	[147,161,162]
Thermochemical conversion of carbonaceous feedstocks	Gasification	Gasification	Biomass waste [1]	H_2 + syngas	800–2000 °C	Fluidized-bed and fixed-bed reactors	[109,111]
Thermochemical conversion of carbonaceous feedstocks	Hydrothermal gasification	Supercritical water gasification	Biomass waste [1]	H_2 + CO_2	374–500 °C (Water pressure >25 MPa)	Heat exchangers	[121,122]
Thermochemical conversion of carbonaceous feedstocks	Hydrothermal liquefaction	Hydrothermal liquefaction	Wet biomass waste	Bio-oil	75–250 °C (Water pressure 1.5–10 MPa)	Heat exchangers	[141,142]
Thermochemical conversion of carbonaceous feedstocks	Biomass pyrolysis	Slow pyrolysis	Biomass waste	Biochar (50–70%), bio-oil (20–30%), and syngas (10–20%)	200–400 °C	One-stage pyrolysis process characterized by slow pyrolysis process (5 to 30 min)	[130]
Thermochemical conversion of carbonaceous feedstocks	Biomass pyrolysis	Intermediate pyrolysis	Biomass waste	Biochar (20–30%), bio-oil (50–70%), and syngas (10–20%)	400–600 °C	One-stage pyrolysis process characterized by intermediate pyrolysis process (1 to 5 min)	[130]
Thermochemical conversion of carbonaceous feedstocks	Biomass pyrolysis	Fast or flash pyrolysis	Biomass waste	Biochar (15–40%), bio-oil (15–20%), and syngas (50–70%)	600–1000 °C	One-stage pyrolysis process characterized by fast pyrolysis (<2 s) or flash pyrolysis (<1 s)	[163,164]

[1] Such as corn stover, sugarcane bagasse, straw, saw mill, etc.

Table 7. Remarks on the use of MS mixtures in processes for the production of hydrogen and syngas.

Process Class	Process Family	Process	MS Mixture (T_{freeze}-T_{max})	MS Interface
Steam electrolysis	Solid oxide steam electrolysis	Solid oxide steam electrolysis	Quaternary mixtures (coupling with CSP plants using solar salt requires intermediate HTF)	Steam generator, with the possibility of using salts from cold tank
Steam electrolysis	Molten carbonate steam electrolysis	Molten carbonate steam electrolysis	Quaternary mixtures (coupling with CSP plants using solar salt requires intermediate HTF)	Steam generator (and amine regeneration column reboilers, if included), with the possibility of using salts from cold tank
Thermo(-electro-) chemical cycles	Sulfur-family cycles	Sulfur-family cycles	Solar salt (240–565 °C). In the future, chlorides or other very-high-temperature mixtures could be used.	Sulfuric acid concentration reboilers (~200 °C), sulfuric acid vaporization, and decomposition exchanger–reactor (300–500 °C)
Thermo(-electro-) chemical cycles	Sulfur-family cycles	Hybrid sulfur (Westinghouse) cycle	Solar salt (240–565 °C). In the future, chlorides or other very-high-temperature mixtures could be used.	Sulfuric acid concentration reboilers (~200 °C), sulfuric acid vaporization, and decomposition exchanger–reactor (300–500 °C)
Thermo(-electro-) chemical cycles	Sulfur-family cycles	Sulphur–iodine cycle	Solar salt (240–565 °C). In the future, chlorides or other very-high-temperature mixtures could be used.	Sulfuric acid concentration reboilers (~200 °C), sulfuric acid vaporization, decomposition exchanger–reactor (300–500 °C) and separation of HI from I2, followed by HI cracking (endothermic, at 300–450 °C)
Thermo(-electro-) chemical cycles	Sulfur-family cycles	S-A cycle	Solar Salt (240–565 °C). In the future, chlorides or other very-high-temperature mixtures could be used.	Sulfuric acid concentration reboilers (~200 °C), sulfuric acid vaporization, decomposition exchanger–reactor (300–500 °C), and ammonium sulfate decomposition (400–500 °C)
Thermo(-electro-) chemical cycles	Sulfur-family cycles	Modified S-A cycle	Solar Salt (240–565 °C). In the future, chlorides or other very-high-temperature mixtures could be used.	Dehydration of metal sulfate (350–450 °C), and ammonium sulfate decomposition (400–500 °C)

Table 7. *Cont.*

Process Class	Process Family	Process	MS Mixture (T_{freeze}-T_{max})	MS Interface
Thermo(-electro-) chemical cycles	Sulfur-family cycles	Modified sulfur–iodine with solid intermediates	Solar salt (240–565 °C). In the future, chlorides or other very-high-temperature mixtures could be used.	Metal sulfate Pre-heating and dehydration (up to 500 °C) and Metal iodide pre-heating and dehydration (up to 500 °C)
Thermo(-electro-) chemical cycles	Non-volatile metal oxide cycles	Non-volatile metal oxide cycles	Solar salt (240–565 °C)	MSs could be considered for heat recovery/thermal buffering/reactant pre-heating in some parts of the plant
Thermo(-electro-) chemical cycles	Non-volatile metal oxide cycles	Mixed ferrites	In the future, chlorides or other very-high-temperature mixtures could be used	MSs could be considered for H_2/CO_2 separation from excess water
Thermo(-electro-) chemical cycles	Metal halide-based hybrid cycles	UT-3	In the future, chlorides or other very-high-temperature mixtures could be used	MSs could be considered for pre-heating regarding water splitting with HBr formation and hydrogen formation from $FeBr_2$
Thermo(-electro-) chemical cycles	Metal halide-based hybrid cycles	Cu-Cl cycle	Solar salt (240–565 °C)	Reactor for oxygen production at 530 °C (configuration to be defined, e.g., jacketed reactor, integrated heat exchanger/coil, etc.)
Thermochemical conversion of carbonaceous feedstocks	Steam reforming	Low-temperature steam methane (or biogas) reforming	Solar salt (240–565 °C)	Heat exchangers, steam generators, and integrated membrane reactors/heat exchangers
Thermochemical conversion of carbonaceous feedstocks	Gasification	Gasification	Solar salt (240–565 °C). In the future, chlorides or other very-high-temperature mixtures could be used.	MSs could be considered for feeding the reactions in the pyrolysis step (temperature of up to 500 °C) in down-draft reactors
Thermochemical conversion of carbonaceous feedstocks	Hydrothermal gasification	Supercritical water gasification	Solar salt (240–565 °C)	Heat exchangers and steam generators

Table 7. *Cont.*

Process Class	Process Family	Process	MS Mixture (T_{freeze}-T_{max})	MS Interface
Thermochemical conversion of carbonaceous feedstocks	Hydrothermal liquefaction	Hydrothermal liquefaction	Ternary mixtures	Heat exchangers
Thermochemical conversion of carbonaceous feedstocks	Biomass pyrolysis	Slow pyrolysis	Solar salt (240–565 °C)	Heat exchangers, steam generators, and integrated membrane reactors/heat exchangers
Thermochemical conversion of carbonaceous feedstocks	Biomass pyrolysis	Intermediate pyrolysis	Solar salt (240–565 °C)	Heat exchangers, steam generators, and integrated membrane reactors/heat exchangers
Thermochemical conversion of carbonaceous feedstocks	Biomass pyrolysis	Fast or flash pyrolysis	In the future, chlorides or other very-high-temperature mixtures could be used	Heat exchangers and integrated membrane reactors/heat exchangers

7. Conclusions

In this review, extensive investigations were focused on detailed studies on molten salt mixtures and electrochemical and thermochemical processes for hydrogen and syngas production.

This research provides a detailed overview of available molten salt mixtures and their thermophysical properties, with a particular focus on their application in thermo-electrochemical processes. Among the various alternatives, nitrate-based (binary and ternary) salt mixtures are a conventional choice for numerous applications and emerge first as the most promising option for thermochemical applications. On the other hand, quaternary, quinary, and senary reciprocal mixtures, characterized by low melting temperatures (from 90 °C down to 56 °C), are appropriate for low-temperature applications; whereas for high temperatures (more than 600 °C), chloride and fluoride mixtures can be used, but with regard to corrosion, they present particularly severe issues and demand high costs.

This work also reviewed three main types of processes employed for hydrogen and syngas production: thermochemical processes, which include conventional methods, such as thermolysis or steam reforming, cracking, and gasification of carbonaceous feedstocks; electrochemical processes, predominantly involving the electrolysis of water; and hybrid processes, like electrolysis of steam and hybrid sulfur cycles. Therefore, for each process, the use of a specific type of molten salt was proposed based on the operating conditions of the cycle.

In this analysis, it has been pointed out that solar salt and the ternary nitrate-based mixture can mainly feed the processes of gasification, supercritical water gasification, slow and intermediate pyrolysis, and hydrothermal liquefaction, where heat between 200 and 500 °C is required. With appropriate process modifications, solar salt can supply heat at 550 °C for the steam reforming process. Among the thermochemical processes, molten salt mixtures can only be used to supply heat at specific steps, such as the hydriodic acid decomposition (endothermic stage at 300–450 °C) in the sulfur–iodine cycle and the thermolysis step (endothermic step at 530 °C) in the Cu-Cl cycle.

In conclusion, this research represents a milestone for future work directed towards developing a ground-breaking concept for molten salt-driven hydrogen and syngas production. The aim is to utilize molten salts as a dynamic interface for the continuous delivery of high-temperature renewable heat from multiple sources, thereby advancing the state of the art in industrial hydrogen and syngas processes. This novel approach promises to reshape the landscape of sustainable energy production, enhancing efficiency and reducing carbon footprints across various sectors. This study's insights are pivotal for the development of molten salt-based energy storage systems. Such systems are envisioned as crucial, scalable, and sustainable interconnection elements between different energy sources, consistent with the EU's long-term objectives for energy security and environmental sustainability. Consequently, future research activities should concentrate on creating flexible interconnections that link renewable power generation and distribution, the electricity grid, and the gas grid. This will facilitate the generation of electricity, the provision of renewable heat at medium and high temperatures, and the production of renewable fuels, leading to enhanced dispatchability and resilience within interconnected energy networks.

Author Contributions: Conceptualization, L.T., P.H. and M.L.; methodology, M.D., L.T., P.H. and M.L.; investigation, M.D., A.C.T., F.R., S.S., L.T., D.C. and J.M.; data curation, M.D., S.S., A.C.T. and D.C.; writing—original draft preparation, M.D., A.C.T., F.R., S.S., L.T., D.C. and J.M.; writing—review and editing, F.R. and M.D.; supervision, S.S., L.T., P.H. and M.L.; project administration, M.D. and P.H.; funding acquisition, P.H. All authors have read and agreed to the published version of the manuscript.

Funding: This work was supported by the SALTOpower project (European Twinning for research in Molten Salt Technology to Power and Energy System Applications), funded by the EU within the Horizon Europe Research & Innovation Programme, grant agreement no: 101079303.

Conflicts of Interest: The authors declare no conflicts of interest.

References

1. European Commission the European Green Deal. Available online: https://commission.europa.eu/strategy-and-policy/priorities-2019-2024/european-green-deal_en (accessed on 11 June 2024).
2. European Commission Fit for 55: Delivering on the Proposals. Available online: https://commission.europa.eu/strategy-and-policy/priorities-2019-2024/european-green-deal/delivering-european-green-deal/fit-55-delivering-proposals_en (accessed on 11 June 2024).
3. European Commission. Next Generation EU. Available online: https://next-generation-eu.europa.eu/index_en (accessed on 11 June 2024).
4. European Commission. *REPowerEU*; European Commission: Brussels, Belgium, 2022.
5. European Commission. Directive-EU-2023/2413-EN-Renewable Energy Directive-EUR-Lex. Available online: https://eur-lex.europa.eu/legal-content/EN/TXT/?uri=CELEX:32023L2413 (accessed on 11 June 2024).
6. Bhandari, R.; Adhikari, N. A Comprehensive Review on the Role of Hydrogen in Renewable Energy Systems. *Int. J. Hydrogen Energy* **2024**, *82*, 923–951. [CrossRef]
7. Ajanovic, A.; Sayer, M.; Haas, R. On the Future Relevance of Green Hydrogen in Europe. *Appl. Energy* **2024**, *358*, 122586. [CrossRef]
8. Islam, A.; Islam, T.; Mahmud, H.; Raihan, O.; Islam, M.S.; Marwani, H.M.; Rahman, M.M.; Asiri, A.M.; Hasan, M.M.; Hasan, M.N.; et al. Accelerating the Green Hydrogen Revolution: A Comprehensive Analysis of Technological Advancements and Policy Interventions. *Int. J. Hydrogen Energy* **2024**, *67*, 458–486. [CrossRef]
9. Majewski, S.; Zhao, X.; Vivanco-Martín, B.; Iranzo, A. Analysis of the European Strategy for Hydrogen: A Comprehensive Review. *Energies* **2023**, *16*, 3866. [CrossRef]
10. Nunes, V.M.B.; Queirós, C.S.; Lourenço, M.J.V.; Santos, F.J.V.; Nieto de Castro, C.A. Molten Salts as Engineering Fluids—A Review: Part I. Molten Alkali Nitrates. *Appl. Energy* **2016**, *183*, 603–611. [CrossRef]
11. Bernagozzi, M.; Panesar, A.S.; Morgan, R. Molten Salt Selection Methodology for Medium Temperature Liquid Air Energy Storage Application. *Appl. Energy* **2019**, *248*, 500–511. [CrossRef]
12. Caraballo, A.; Galán-Casado, S.; Caballero, Á.; Serena, S. Molten Salts for Sensible Thermal Energy Storage: A Review and an Energy Performance Analysis. *Energies* **2021**, *14*, 1197. [CrossRef]
13. Myers, P.D.; Goswami, D.Y. Thermal Energy Storage Using Chloride Salts and Their Eutectics. *Appl. Therm. Eng.* **2016**, *109*, 889–900. [CrossRef]
14. Sau, S.; Corsaro, N.; Crescenzi, T.; D'Ottavi, C.; Liberatore, R.; Licoccia, S.; Russo, V.; Tarquini, P.; Tizzoni, A.C.; D'Ottavi, C.; et al. Techno-Economic Comparison between CSP Plants Presenting Two Different Heat Transfer Fluids. *Appl. Energy* **2016**, *168*, 96–109. [CrossRef]
15. Roper, R.; Harkema, M.; Sabharwall, P.; Riddle, C.; Chisholm, B.; Day, B.; Marotta, P. Molten Salt for Advanced Energy Applications: A Review. *Ann. Nucl. Energy* **2022**, *169*, 108924. [CrossRef]
16. Bhatnagar, P.; Siddiqui, S.; Sreedhar, I.; Parameshwaran, R. Molten Salts: Potential Candidates for Thermal Energy Storage Applications. *Int. J. Energy Res.* **2022**, *46*, 17755–17785. [CrossRef]
17. Vignarooban, K.; Xu, X.; Arvay, A.; Hsu, K.; Kannan, A.M. Heat Transfer Fluids for Concentrating Solar Power Systems—A Review. *Appl. Energy* **2015**, *146*, 383–396. [CrossRef]
18. Collares-Pereira, M.; Canavarro, D.; Guerreiro, L.L. Linear Fresnel Reflector (LFR) Plants Using Superheated Steam, Molten Salts, and Other Heat Transfer Fluids. In *Advances in Concentrating Solar Thermal Research and Technology*; Elsevier: Amsterdam, The Netherlands, 2017; pp. 339–352. ISBN 9780081005170.
19. Laing, D.; Bauer, T.; Breidenbach, N.; Hachmann, B.; Johnson, M. Development of High Temperature Phase-Change-Material Storages. *Appl. Energy* **2013**, *109*, 497–504. [CrossRef]
20. Fiorucci, L.C.; Goldstein, S.L.; Fiorucci, L.C.; Goldstein, S.L. Manufacture, Distribution, and Handling of Nitrate Salts for Solar-Thermal Applications. *STIN* **1982**, *83*, 21625.
21. Bradshaw, R.W.; Siegel, N.P. Molten Nitrate Salt Development for Thermal Energy Storage in Parabolic Trough Solar Power Systems. In Proceedings of the ASME 2008 2nd International Conference on Energy Sustainability Collocated with the Heat Transfer, Fluids Engineering, and 3rd Energy Nanotechnology Conferences, Jacksonville, FL, USA, 10–14 August 2008; Volume 2, pp. 631–637.

22. Delise, T.; Tizzoni, A.C.; Ferrara, M.; Corsaro, N.; D'Ottavi, C.; Sau, S.; Licoccia, S. Thermophysical, Environmental, and Compatibility Properties of Nitrate and Nitrite Containing Molten Salts for Medium Temperature CSP Applications: A Critical Review. *J. Eur. Ceram. Soc.* **2019**, *39*, 92–99. [CrossRef]
23. Jriri, T.; Rogez, J.; Bergman, C.; Mathieu, J.C. Thermodynamic Study of the Condensed Phases of $NaNO_3$, KNO_3 and $CsNO_3$ and Their Transitions. *Thermochim. Acta* **1995**, *266*, 147–161. [CrossRef]
24. Bauer, T.; Pfleger, N.; Breidenbach, N.; Eck, M.; Laing, D.; Kaesche, S. Material Aspects of Solar Salt for Sensible Heat Storage. *Appl. Energy* **2013**, *111*, 1114–1119. [CrossRef]
25. Wu, Y.; Li, Y.; Ren, N.; Ma, C. Improving the Thermal Properties of $NaNO_3$-KNO_3 for Concentrating Solar Power by Adding Additives. *Sol. Energy Mater. Sol. Cells* **2017**, *160*, 263–268. [CrossRef]
26. Bonk, A.; Sau, S.; Uranga, N.; Hernaiz, M.; Bauer, T. Advanced Heat Transfer Fluids for Direct Molten Salt Line-Focusing CSP Plants. *Prog. Energy Combust. Sci.* **2018**, *67*, 69–87. [CrossRef]
27. Bradshaw, R.W.W.; Meeker, D.E.E. High-Temperature Stability of Ternary Nitrate Molten Salts for Solar Thermal Energy Systems. *Sol. Energy Mater.* **1990**, *21*, 51–60. [CrossRef]
28. Raade, J.W.; Padowitz, D. Development of Molten Salt Heat Transfer Fluid With Low Melting Point and High Thermal Stability. *J. Sol. Energy Eng.* **2011**, *133*, 031013. [CrossRef]
29. Li, X.; Xie, L. Experimental Investigation and Thermodynamic Modeling of the $LiNO_3$-$RbNO_3$-$AgNO_3$ System and Its Subsystems. *J. Alloys Compd.* **2018**, *736*, 124–135. [CrossRef]
30. Vallet, C. Phase Diagrams and Thermodynamic Properties of Some Molten Nitrate Mixtures. *J. Chem. Thermodyn.* **1972**, *4*, 105–114. [CrossRef]
31. Bauer, T.; Pfleger, N.; Laing, D.; Steinmann, W.-D.; Eck, M.; Kaesche, S. High-Temperature Molten Salts for Solar Power Application. In *Molten Salts Chemistry*; Elsevier: Amsterdam, The Netherlands, 2013; pp. 415–438. ISBN 9780123985385.
32. Ding, W.; Bauer, T. Progress in Research and Development of Molten Chloride Salt Technology for Next Generation Concentrated Solar Power Plants. *Engineering* **2021**, *7*, 334–347. [CrossRef]
33. Gomez, J.C. *High-Temperature Phase Change Materials (PCM) Candidates for Thermal Energy Storage (TES) Applications*; NREL: Golden, CO, USA, 2011; Volume 303.
34. Misra, A.K.; Whittenberger, J.D. Fluoride Salts and Container Materials for Thermal Energy Storage Applications in the Temperature Range 973–1400 K. In Proceedings of the 22nd Intersociety Energy Conversion Engineering Conference, Reston, VA, USA, 10 August 1987.
35. Vidal, J.C.; Klammer, N. Molten Chloride Technology Pathway to Meet the U.S. DOE Sunshot Initiative with Gen3 CSP. In Proceedings of the AIP Conference Proceedings, Bodrum, Turkey, 25 July 2019; Volume 2126, p. 080006.
36. Tripi, V.; Sau, S.; Tizzoni, A.C.; Mansi, E.; Spadoni, A.; Corsaro, N.; D'Ottavi, C.; Capocelli, M.; Licoccia, S.; Delise, T. A General Thermodynamic Model for Eutectics of Phase Change Molten Salts in Concentrating Solar Power Applications. *J. Energy Storage* **2021**, *33*, 102065. [CrossRef]
37. Hosoya, Y.; Terai, T.; Yoneoka, T.; Tanaka, S. Compatibility of Structural Materials with Molten Chloride Mixture at High Temperature. *J. Nucl. Mater.* **1997**, *248*, 348–353. [CrossRef]
38. Jantzen, C.A. *An Investigation of Primary Circuit Materials in Molten Chloride Salts with the Design of High Temperature Corrosion Vessels*; The University of Manchester: Manchester, UK, 2019.
39. Kruizenga, A. *Corrosion Mechanisms in Chloride and Carbonate Salts*; Sandia National Laboratories: Albuquerque, NM, USA; Livermore, CA, USA, 2012.
40. Villada, C.; Ding, W.; Bonk, A.; Bauer, T. Engineering Molten $MgCl_2$–KCl–NaCl Salt for High-Temperature Thermal Energy Storage: Review on Salt Properties and Corrosion Control Strategies. *Sol. Energy Mater. Sol. Cells* **2021**, *232*, 111344. [CrossRef]
41. Huang, Q.; Lu, G.; Wang, J.; Yu, J. Thermal Decomposition Mechanisms of $MgCl_2 \cdot 6H_2O$ and $MgCl_2 \cdot H_2O$. *J. Anal. Appl. Pyrolysis* **2011**, *91*, 159–164. [CrossRef]
42. Yin, H.; Wang, Z.; Lai, X.; Wang, Y.; Tang, Z. Optimum Design and Key Thermal Property of NaCl–KCl–CaC_{l2} Eutectic Salt for Ultra-High-Temperature Thermal Energy Storage. *Sol. Energy Mater. Sol. Cells* **2022**, *236*, 111541. [CrossRef]
43. Kruizenga, A.M.; Andraka, C.E.; Kolb, W.J. *Molten Salt Technology*; Sandia National Laboratories: Albuquerque, NM, USA; Livermore, CA, USA, 2016.
44. Mahboob, K.; Khan, A.A.; Khan, M.A.; Sarwar, J.; Khan, T.A. Comparison of Li_2CO_3-Na_2CO_3-K_2CO_3, KCl-$MgCl_2$ and $NaNO_3$-KNO_3 as Heat Transfer Fluid for Different SCO_2 and Steam Power Cycles in CSP Tower Plant under Different DNI Conditions. *Adv. Mech. Eng.* **2021**, *13*, 168781402110119. [CrossRef]
45. Prieto, C.; Fereres, S.; Ruiz-Cabañas, F.J.; Rodriguez-Sanchez, A.; Montero, C. Carbonate Molten Salt Solar Thermal Pilot Facility: Plant Design, Commissioning and Operation up to 700 °C. *Renew. Energy* **2020**, *151*, 528–541. [CrossRef]
46. Li, Q.; Li, C.; Du, Z.; Jiang, F.; Ding, Y. A Review of Performance Investigation and Enhancement of Shell and Tube Thermal Energy Storage Device Containing Molten Salt Based Phase Change Materials for Medium and High Temperature Applications. *Appl. Energy* **2019**, *255*, 113806. [CrossRef]

47. Sau, G.S.; Tripi, V.; Tizzoni, A.C.; Liberatore, R.; Mansi, E.; Spadoni, A.; Corsaro, N.; Capocelli, M.; Delise, T.; Della Libera, A. High-Temperature Chloride-Carbonate Phase Change Material: Thermal Performances and Modelling of a Packed Bed Storage System for Concentrating Solar Power Plants. *Energies* **2021**, *14*, 5339. [CrossRef]
48. Dunlop, T.O.; Jarvis, D.J.; Voice, W.E.; Sullivan, J.H. Stabilization of Molten Salt Materials Using Metal Chlorides for Solar Thermal Storage. *Sci. Rep.* **2018**, *8*, 8190. [CrossRef]
49. Zavoico, A.B. *Solar Power Tower Design Basis Document, Revision 0*; Sandia National Laboratories: Albuquerque, NM, USA; Livermore, CA, USA, 2001.
50. Boerema, N.; Morrison, G.; Taylor, R.; Rosengarten, G. Liquid Sodium versus Hitec as a Heat Transfer Fluid in Solar Thermal Central Receiver Systems. *Sol. Energy* **2012**, *86*, 2293–2305. [CrossRef]
51. Serrano-López, R.; Fradera, J.; Cuesta-López, S. Molten Salts Database for Energy Applications. *Chem. Eng. Process. Process Intensif.* **2013**, *73*, 87–102. [CrossRef]
52. Zhao, C.Y.; Wu, Z.G. Thermal Property Characterization of a Low Melting-Temperature Ternary Nitrate Salt Mixture for Thermal Energy Storage Systems. *Sol. Energy Mater. Sol. Cells* **2011**, *95*, 3341–3346. [CrossRef]
53. Siegel, N.P.; Bradshaw, R.W.; Cordaro, J.B.; Kruizenga, A.M. Thermophysical Property Measurement of Nitrate Salt Heat Transfer Fluids. In Proceedings of the ASME 2011 5th International Conference on Energy Sustainability, Parts A, B and C, Washington, DC, USA, 7–10 August 2011; pp. 439–446.
54. Wang, T.; Mantha, D.; Reddy, R.G. Thermal Stability of the Eutectic Composition in $LiNO_3$–$NaNO_3$–KNO_3 Ternary System Used for Thermal Energy Storage. *Sol. Energy Mater. Sol. Cells* **2012**, *100*, 162–168. [CrossRef]
55. Coscia, K.; Nelle, S.; Elliott, T.; Mohapatra, S.; Oztekin, A.; Neti, S. Thermophysical Properties of $LiNO_3$–$NaNO_3$–KNO_3 Mixtures for Use in Concentrated Solar Power. *J. Sol. Energy Eng.* **2013**, *135*, 034506. [CrossRef]
56. Roget, F.; Favotto, C.; Rogez, J. Study of the KNO_3–$LiNO_3$ and KNO_3–$NaNO_3$–$LiNO_3$ Eutectics as Phase Change Materials for Thermal Storage in a Low-Temperature Solar Power Plant. *Sol. Energy* **2013**, *95*, 155–169. [CrossRef]
57. Peng, Q.; Ding, J.; Wei, X.; Jiang, G. Thermodynamic Investigation of the Eutectic Mixture of the $LiNO_3$–$NaNO_3$–KNO_3 $Ca(NO_3)_2$ System. *Int. J. Thermophys.* **2017**, *38*, 142. [CrossRef]
58. Jiang, Z.; Leng, G.; Ye, F.; Ge, Z.; Liu, C.; Wang, L.; Huang, Y.; Ding, Y. Form-Stable $LiNO_3$–$NaNO_3$–KNO_3–$Ca(NO_3)_2$/Calcium Silicate Composite Phase Change Material (PCM) for Mid-Low Temperature Thermal Energy Storage. *Energy Convers. Manag.* **2015**, *106*, 165–172. [CrossRef]
59. Cordaro, J.G.; Rubin, N.C.; Bradshaw, R.W. Multicomponent Molten Salt Mixtures Based on Nitrate/Nitrite Anions. *J. Sol. Energy Eng.* **2011**, *133*, 011014. [CrossRef]
60. Wang, T.; Mantha, D.; Reddy, R.G. Novel Low Melting Point Quaternary Eutectic System for Solar Thermal Energy Storage. *Appl. Energy* **2013**, *102*, 1422–1429. [CrossRef]
61. Li, Y.; Xu, X.; Wang, X.; Li, P.; Hao, Q.; Xiao, B. Survey and Evaluation of Equations for Thermophysical Properties of Binary/Ternary Eutectic Salts from NaCl, KCl, $MgCl_2$, $CaCl_2$, $ZnCl_2$ for Heat Transfer and Thermal Storage Fluids in CSP. *Sol. Energy* **2017**, *152*, 57–79. [CrossRef]
62. Li, P.; Molina, E.; Wang, K.; Xu, X.; Dehghani, G.; Kohli, A.; Hao, Q.; Kassaee, M.H.; Jeter, S.M.; Teja, A.S. Thermal and Transport Properties of NaCl–KCl–ZnCl2 Eutectic Salts for New Generation High-Temperature Heat-Transfer Fluids. *J. Sol. Energy Eng.* **2016**, *138*, 054501. [CrossRef]
63. Xu, X.; Wang, X.; Li, P.; Li, Y.; Hao, Q.; Xiao, B.; Elsentriecy, H.; Gervasio, D. Experimental Test of Properties of KCl–$MgCl_2$ Eutectic Molten Salt for Heat Transfer and Thermal Storage Fluid in Concentrated Solar Power Systems. *J. Sol. Energy Eng.* **2018**, *140*, 051011. [CrossRef]
64. Wei, X.; Song, M.; Wang, W.; Ding, J.; Yang, J. Design and Thermal Properties of a Novel Ternary Chloride Eutectics for High-Temperature Solar Energy Storage. *Appl. Energy* **2015**, *156*, 306–310. [CrossRef]
65. Du, L.; Tian, H.; Wang, W.; Ding, J.; Wei, X.; Song, M. Thermal Stability of the Eutectic Composition in NaCl-$CaCl_2$-$MgCl_2$ Ternary System Used for Thermal Energy Storage Applications. *Energy Procedia* **2017**, *105*, 4185–4191. [CrossRef]
66. Du, L.; Ding, J.; Tian, H.; Wang, W.; Wei, X.; Song, M. Thermal Properties and Thermal Stability of the Ternary Eutectic Salt NaCl-$CaCl_2$-$MgCl_2$ Used in High-Temperature Thermal Energy Storage Process. *Appl. Energy* **2017**, *204*, 1225–1230. [CrossRef]
67. Xu, X.; Dehghani, G.; Ning, J.; Li, P. Basic Properties of Eutectic Chloride Salts NaCl-KCl-$ZnCl_2$ and NaCl-KCl-$MgCl_2$ as HTFs and Thermal Storage Media Measured Using Simultaneous DSC-TGA. *Sol. Energy* **2018**, *162*, 431–441. [CrossRef]
68. Forsberg, C.W.; Peterson, P.F.; Zhao, H. High-Temperature Liquid-Fluoride-Salt Closed-Brayton-Cycle Solar Power Towers. *J. Sol. Energy Eng.* **2007**, *129*, 141–146. [CrossRef]
69. Williams, D.F.; Toth, L.M.; Clarno, K.T. *Assessment of Candidate Molten Salt Coolants for the Advanced High-Temperature Reactor (AHTR)*; Brookhaven National Laboratory: Appleton, NY, USA, 2006.
70. Jerden, J. *Molten Salt Thermophysical Properties Database Development: 2019 Update Chemical and Fuel Cycle Technologies Division*; Argonne National Laboratory: Argonne, IL, USA, 2019.

71. An, X.-H.; Cheng, J.-H.; Su, T.; Zhang, P. Determination of Thermal Physical Properties of Alkali Fluoride/Carbonate Eutectic Molten Salt. In Proceedings of the AIP Conference Proceedings, Abu Dhab, United Arab Emirates, 27 June 2017; Volume 1850, p. 070001.
72. Giaconia, A.; Tizzoni, A.C.; Sau, S.; Corsaro, N.; Mansi, E.; Spadoni, A.; Delise, T. Assessment and Perspectives of Heat Transfer Fluids for CSP Applications. *Energies* **2021**, *14*, 7486. [CrossRef]
73. Delise, T.; Tizzoni, A.C.C.; Menale, C.; Telling, M.T.F.; Bubbico, R.; Crescenzi, T.; Corsaro, N.; Sau, S.; Licoccia, S. Technical and Economic Analysis of a CSP Plant Presenting a Low Freezing Ternary Mixture as Storage and Transfer Fluid. *Appl. Energy* **2020**, *265*, 114676. [CrossRef]
74. Villada, C.; Bonk, A.; Bauer, T.; Bolívar, F. High-Temperature Stability of Nitrate/Nitrite Molten Salt Mixtures under Different Atmospheres. *Appl. Energy* **2018**, *226*, 107–115. [CrossRef]
75. Kruizenga, A.; Cordaro, J.G. *Preliminary Development of Thermal Stability Criterion for Alkali Nitrates*; Sandia National Laboratories: Albuquerque, NM, USA; Livermore, CA, USA, 2011.
76. Freeman, E.S. The Kinetics of the Thermal Decomposition of Potassium Nitrate and of the Reaction between Potassium Nitrite and Oxygen. *J. Am. Chem. Soc.* **1957**, *79*, 838–842. [CrossRef]
77. Freeman, E.S. The Kinetics of the Thermal Decomposition of Sodium Nitrate and of the Reaction between Sodium Nitrite and Oxygen. *J. Phys. Chem.* **1956**, *60*, 1487–1493. [CrossRef]
78. Steinbrecher, J.; Braun, M.; Bauer, T.; Kunkel, S.; Bonk, A. Solar Salt above 600 °C: Impact of Experimental Design on Thermodynamic Stability Results. *Energies* **2023**, *16*, 5241. [CrossRef]
79. Steinbrecher, J.; Hanke, A.; Braun, M.; Bauer, T.; Bonk, A. Stabilization of Solar Salt at 650 °C—Thermodynamics and Practical Implications for Thermal Energy Storage Systems. *Sol. Energy Mater. Sol. Cells* **2023**, *258*, 112411. [CrossRef]
80. Kust, R.N.; Burke, J.D. Thermal Decomposition in Alkali Metal Nitrate Melts. *Inorg. Nucl. Chem. Lett.* **1970**, *6*, 333–335. [CrossRef]
81. Wang, J.; Jiang, Y.; Ni, Y.; Wu, A.; Li, J. Investigation on Static and Dynamic Corrosion Behaviors of Thermal Energy Transfer and Storage System Materials by Molten Salts in Concentrating Solar Power Plants. *Mater. Corros.* **2019**, *70*, 102–109. [CrossRef]
82. *International Renewable Energy Agency Renewable Energy Statistics 2018*; IRENA: Masdar, United Arab Emirates, 2018.
83. Bertuccioli, L.; Chan, A.; Hart, D.; Lehner, F.; Madden, B.; Standen, E. *Fuel Cells and Hydrogen Joint Undertaking Development of Water Electrolysis in the European Union Final Report*; New Energy World: London, UK, 2014; pp. 68–69.
84. Sattler, C.; Monnerie, N.; Houaijia, A.; Romero, M.; Aguilar, J.G.; Miguel, A.; Reyes, L.; Turchetti, L.; Giaconia, A.; Mazzei, D.; et al. *Scientific and Technological Alliance for Guaranteeing the European Excellence in Concentrating Solar Thermal Energy D9.4: Final Report on "Technology Roadmap for Solar Fuels"*; EERA: Berlin, Germany, 2014.
85. Compact Multifuel-Energy to Hydrogen Converter | CoMETHy | Project | News & Multimedia | FP7 | CORDIS | European Commission. Available online: https://cordis.europa.eu/project/id/279075 (accessed on 6 June 2024).
86. *Fuel Cells and Hydrogen Joint Undertaking (Fch Ju) Multi-Annual Work Plan*; New Energy World: London, UK, 2014.
87. Fujiwara, S.; Kasai, S.; Yamauchi, H.; Yamada, K.; Makino, S.; Matsunaga, K.; Yoshino, M.; Kameda, T.; Ogawa, T.; Momma, S.; et al. Hydrogen Production by High Temperature Electrolysis with Nuclear Reactor. *Prog. Nucl. Energy* **2008**, *50*, 422–426. [CrossRef]
88. Sunfire Electrolyzers-Sunfire. Available online: https://www.sunfire.de/en/hydrogen (accessed on 10 June 2024).
89. Badwal, S.P.S.; Giddey, S.S.; Munnings, C.; Bhatt, A.I.; Hollenkamp, A.F. Emerging Electrochemical Energy Conversion and Storage Technologies. *Front. Chem.* **2014**, *2*, 79. [CrossRef] [PubMed]
90. Safari, F.; Dincer, I. A Review and Comparative Evaluation of Thermochemical Water Splitting Cycles for Hydrogen Production. *Energy Convers. Manag.* **2020**, *205*, 112182. [CrossRef]
91. Liberatore, R.; Caputo, G.; Felici, C.; Spadona, A. Demonstration of Hydrogen Production by the Sulphur-Iodine Cycle: Realization of a 10 NL/h Plant. In Proceedings of the 18th World Hydrogen Energy Conference 2010, WHEC 2010 Proceedings, Essen, Germany, 16–21 May 2010; Volume 2, pp. 295–300.
92. Liberatore, R.; Lanchi, M.; Giaconia, A.; Tarquini, P. Energy and Economic Assessment of an Industrial Plant for the Hydrogen Production by Water-Splitting through the Sulfur-Iodine Thermochemical Cycle Powered by Concentrated Solar Energy. *Int. J. Hydrogen Energy* **2012**, *37*, 9550–9565. [CrossRef]
93. Prosini, P.P.; Cento, C.; Giaconia, A.; Caputo, G.; Sau, S. A Modified Sulphur-Iodine Cycle for Efficient Solar Hydrogen Production. *Int. J. Hydrogen Energy* **2009**, *34*, 1218–1225. [CrossRef]
94. Lanchi, M.; Varsano, F.; Brunetti, B.; Murmura, M.A.; Annesini, M.C.; Turchetti, L.; Grena, R. Thermal Characterization of a Cavity Receiver for Hydrogen Production by Thermochemical Cycles Operating at Moderate Temperatures. *Sol. Energy* **2013**, *92*, 256–268. [CrossRef]
95. Parisi, M.; Giaconia, A.; Sau, S.; Spadoni, A.; Caputo, G.; Tarquini, P. Bunsen Reaction and Hydriodic Phase Purification in the Sulfur–Iodine Process: An Experimental Investigation. *Int. J. Hydrogen Energy* **2011**, *36*, 2007–2013. [CrossRef]

96. Liberatore, R.; Cerioli, A.; Lanchi, M.; Spadoni, A.; Tarquini, P. Experimental Vapour–Liquid Equilibrium Data of HI–H2O–I2 Mixtures for Hydrogen Production by Sulphur–Iodine Thermochemical Cycle. *Int. J. Hydrogen Energy* **2008**, *33*, 4283–4290. [CrossRef]
97. Barbarossa, V.; Brutti, S.; Diamanti, M.; Sau, S.; Demeria, G. Catalytic Thermal Decomposition of Sulphuric Acid in Sulphur–Iodine Cycle for Hydrogen Production. *Int. J. Hydrogen Energy* **2006**, *31*, 883–890. [CrossRef]
98. Giaconia, A.; Sau, S.; Felici, C.; Tarquini, P.; Karagiannakis, G.; Pagkoura, C.; Agrafiotis, C.; Konstandopoulos, A.G.; Thomey, D.; De Oliveira, L.; et al. Hydrogen Production via Sulfur-Based Thermochemical Cycles: Part 2: Performance Evaluation of Fe2O3-Based Catalysts for the Sulfuric Acid Decomposition Step. *Int. J. Hydrogen Energy* **2011**, *36*, 6496–6509. [CrossRef]
99. Favuzza, P.; Felici, C.; Lanchi, M.; Liberatore, R.; Mazzocchia, C.V.; Spadoni, A.; Tarquini, P.; Tito, A.C. Decomposition of Hydrogen Iodide in the S–I Thermochemical Cycle over Ni Catalyst Systems. *Int. J. Hydrogen Energy* **2009**, *34*, 4049–4056. [CrossRef]
100. Lanchi, M.; Caputo, G.; Liberatore, R.; Marrelli, L.; Sau, S.; Spadoni, A.; Tarquini, P.; Sau, G.S.; SPADONI, A.; Tarquini, P. Use of Metallic Ni for H2 Production in S–I Thermochemical Cycle: Experimental and Theoretical Analysis. *Int. J. Hydrogen Energy* **2009**, *34*, 1200–1207. [CrossRef]
101. Varsano, F.; Padella, F.; Alvani, C.; Bellusci, M.; La Barbera, A. Chemical Aspects of the Water-Splitting Thermochemical Cycle Based on Sodium Manganese Ferrite. *Int. J. Hydrogen Energy* **2012**, *37*, 11595–11601. [CrossRef]
102. Liberatore, R.; Bassi, A.; Turchetti, L.; Venturin, M. Multi-Objective Optimization of a Hydrogen Production through the HyS Process Powered by Solar Energy in Different Scenarios. *Int. J. Hydrogen Energy* **2018**, *43*, 8683–8697. [CrossRef]
103. Liberatore, R.; Lanchi, M.; Turchetti, L. Hydrogen Production by the Solar-Powered Hybrid Sulfur Process: Analysis of the Integration of the CSP and Chemical Plants in Selected Scenarios. In Proceedings of the AIP Conference Proceedings, Bodrum, Turkey, 25 July 2019; Volume 1734, p. 120006.
104. Turchetti, L.; Liberatore, R.; Sau, S.; Tizzoni, A.C. Carbon-Free Production of Hydrogen via the Solar Powered Hybrid Sulfur Cycle: The SOL2HY2 Project. *Chem. Eng. Trans.* **2015**, *43*, 2179–2184. [CrossRef]
105. Tizzoni, A.C.; Corsaro, N.; D'Ottavi, C.; Licoccia, S.; Sau, S.; Tarquini, P. Oxygen Production by Intermediate Metal Sulphates in Sulphur Based Thermochemical Water Splitting Cycles. *Int. J. Hydrogen Energy* **2015**, *40*, 4065–4083. [CrossRef]
106. Taylor, R.; Davenport, R.; Talbot, J.; Herz, R.; Luc, W.; Genders, D.; Symons, P.; Brown, L. Status of the Solar Sulfur Ammonia Thermochemical Hydrogen Production System for Splitting Water. *Energy Procedia* **2014**, *49*, 2047–2058. [CrossRef]
107. Navarro, R.M.; Peña, M.A.; Fierro, J.L.G. Hydrogen Production Reactions from Carbon Feedstocks: Fossil Fuels and Biomass. *Chem. Rev.* **2007**, *107*, 3952–3991. [CrossRef]
108. Giaconia, A.; Turchetti, L.; Monteleone, G.; Morico, B.; Iaquaniello, G.; Shabtai, K.; Sheintuch, M.; Boettge, D.; Adler, J.; Palma, V.; et al. Development of a Solar-Powered, Fuel-Flexible Compact Steam Reformer: The CoMETHy Project. *Chem. Eng. Trans.* **2013**, *35*, 433–438.
109. Krishna, B.B.; Biswas, B.; Bhaskar, T. Gasification of Lignocellulosic Biomass. In *Biomass, Biofuels, Biochemicals: Biofuels: Alternative Feedstocks and Conversion Processes for the Production of Liquid and Gaseous Biofuels*; Academic Press: Cambridge, MA, USA, 2019; pp. 285–300. ISBN 9780128168561.
110. Yan, M.; Afxentiou, N.; Fokaides, P.A. The State of the Art Overview of the Biomass Gasification Technology. *Curr. Sustain. Energy Rep.* **2021**, *8*, 282–295. [CrossRef]
111. Jha, S.; Okolie, J.A.; Nanda, S.; Dalai, A.K. A Review of Biomass Resources and Thermochemical Conversion Technologies. *Chem. Eng. Technol.* **2022**, *45*, 791–799. [CrossRef]
112. Qian, K.; Kumar, A.; Patil, K.; Bellmer, D.; Wang, D.; Yuan, W.; Huhnke, R.L. Effects of Biomass Feedstocks and Gasification Conditions on the Physiochemical Properties of Char. *Energies* **2013**, *6*, 3972–3986. [CrossRef]
113. Wu, Y.; Yang, W.; Blasiak, W. Energy and Exergy Analysis of High Temperature Agent Gasification of Biomass. *Energies* **2014**, *7*, 2107–2122. [CrossRef]
114. Liu, B.; Ji, S. Comparative Study of Fluidized-Bed and Fixed-Bed Reactor for Syngas Methanation over Ni-W/TiO_2-SiO_2 Catalyst. *J. Energy Chem.* **2013**, *22*, 740–746. [CrossRef]
115. Li, M.; Luo, N.; Lu, Y. Biomass Energy Technological Paradigm (BETP): Trends in This Sector. *Sustainability* **2017**, *9*, 567. [CrossRef]
116. Vivoli, F.P.; Benanti, E. *Energia Dalle Biomasse: Tecnologie e Prospettive*; Regione Siciliana Assessorato Industria: Palermo, Italy, 2008; ISBN 8882861716.
117. Mandl, C.; Obrenberger, I.; Biedermann, F. Updraft-Fixed Bed Gasification of Softwood Bellets: Mathematical Modelling and Comparison with Experimental Data. In Proceedings of the 17th European Biomass Conference and Exhibition, Hamburg, Germany, 29 June–3 July 2009; pp. 1–9.

118. Kruesi, M.; Jovanovic, Z.R.; Steinfeld, A. A Two-Zone Solar-Driven Gasifier Concept: Reactor Design and Experimental Evaluation with Bagasse Particles. *Fuel* **2014**, *117*, 680–687. [CrossRef]
119. Mendonça, M.; Mantilla, V.; Patela, J.; Silva, V.; Resende, F. Design and Experimental Tests of an Imbert Type Downdraft Gasifier Prototype and Clean-up System for Small-Scale Biomass-Based Power Generation. *Renew. Energy Environ. Sustain.* **2022**, *7*, 10. [CrossRef]
120. Pirolisi e Pirogassificazione Delle Biomasse-FitoGen-Università Di Cagliari. Available online: https://sites.unica.it/fitogen/pirolisi-e-pirogassificazione-delle-biomasse/ (accessed on 10 June 2024).
121. Rodriguez Correa, C.; Kruse, A. Supercritical Water Gasification of Biomass for Hydrogen Production—Review. *J. Supercrit. Fluids* **2018**, *133*, 573–590. [CrossRef]
122. Reddy, S.N.; Nanda, S.; Dalai, A.K.; Kozinski, J.A. Supercritical Water Gasification of Biomass for Hydrogen Production. *Int. J. Hydrogen Energy* **2014**, *39*, 6912–6926. [CrossRef]
123. Pandey, A.; Larroche, C.; Ricke, S.; Dussap, C.G.; Gnansounou, E. *Biofuels*; Elsevier: Amsterdam, The Netherlands, 2011. [CrossRef]
124. Davda, R.R.; Shabaker, J.W.; Huber, G.W.; Cortright, R.D.; Dumesic, J.A. A Review of Catalytic Issues and Process Conditions for Renewable Hydrogen and Alkanes by Aqueous-Phase Reforming of Oxygenated Hydrocarbons over Supported Metal Catalysts. *Appl. Catal. B Environ.* **2005**, *56*, 171–186. [CrossRef]
125. Osada, M.; Sato, T.; Watanabe, M.; Shirai, M.; Arai, K. Catalytic Gasification of Wood Biomass in Subcritical and Supercritical Water. *Combust. Sci. Technol.* **2006**, *178*, 537–552. [CrossRef]
126. Elliott, D.C. Catalytic Hydrothermal Gasification of Biomass. *Biofuels Bioprod. Biorefin.* **2008**, *2*, 254–265. [CrossRef]
127. Matsumura, Y.; Minowa, T.; Potic, B.; Kersten, S.R.A.; Prins, W.; Van Swaaij, W.P.M.; Van De Beld, B.; Elliott, D.C.; Neuenschwander, G.G.; Kruse, A.; et al. Biomass Gasification in Near- and Super-Critical Water: Status and Prospects. *Biomass Bioenergy* **2005**, *29*, 269–292. [CrossRef]
128. Chuntanapum, A.; Matsumura, Y. Char Formation Mechanism in Supercritical Water Gasification Process: A Study of Model Compounds. *Ind. Eng. Chem. Res.* **2010**, *49*, 4055–4062. [CrossRef]
129. Wang, A.G.; Austin, D.; Song, H. Catalytic Biomass Valorization. In *Biomass Volume Estimation and Valorization for Energy*; InTech: Singapore, 2017; ISBN 978-953-51-2938-7.
130. Kim, J.S.; Choi, G.G. Pyrolysis of Lignocellulosic Biomass for Biochemical Production. In *Waste Biorefinery Potential Perspect*; Elsevier: Amsterdam, The Netherlands, 2018; pp. 323–348. [CrossRef]
131. Müller, F.L. Solar Reactor Development for Thermochemical Gasification and Calcination Processes. Ph.D. Thesis, ETH Zurich, Zurich, Switzerland, 2018. [CrossRef]
132. Wright, M.M.; Daugaard, D.E.; Satrio, J.A.; Brown, R.C. Techno-Economic Analysis of Biomass Fast Pyrolysis to Transportation Fuels. *Fuel* **2010**, *89*, S2–S10. [CrossRef]
133. Seo, M.W.; Lee, S.H.; Nam, H.; Lee, D.; Tokmurzin, D.; Wang, S.; Park, Y.K. Recent Advances of Thermochemical Conversion Processes for Biorefinery. *Bioresour. Technol.* **2022**, *343*, 126109. [CrossRef]
134. Sánchez-Bastardo, N.; Schlögl, R.; Ruland, H. Response to Comment on "Methane Pyrolysis for Zero-Emission Hydrogen Production: A Potential Bridge Technology from Fossil Fuels to a Renewable and Sustainable Hydrogen Economy". *Ind. Eng. Chem. Res.* **2021**, *60*, 17795–17796. [CrossRef]
135. Devi, M.; Rawat, S. A Comprehensive Review of the Pyrolysis Process: From Carbon Nanomaterial Synthesis to Waste Treatment. *Oxford Open Mater. Sci.* **2021**, *1*, itab014. [CrossRef]
136. Brown, R.C. The Role of Pyrolysis and Gasification in a Carbon Negative Economy. *Processes* **2021**, *9*, 882. [CrossRef]
137. Korányi, T.I.; Németh, M.; Beck, A.; Horváth, A. Recent Advances in Methane Pyrolysis: Turquoise Hydrogen with Solid Carbon Production. *Energies* **2022**, *15*, 6342. [CrossRef]
138. Fan, Z.; Weng, W.; Zhou, J.; Gu, D.; Xiao, W. Catalytic Decomposition of Methane to Produce Hydrogen: A Review. *J. Energy Chem.* **2021**, *58*, 415–430. [CrossRef]
139. McFarland, E. Molten-Salt Methane Pyrolysis Optimization Through in-Situ Carbon Characterization and Reactor Design. Available online: https://arpa-e.energy.gov/programs-and-initiatives/search-all-projects/molten-salt-methane-pyrolysis-optimization-through-situ-carbon-characterization-and-reactor-design (accessed on 6 June 2024).
140. Bhardwaj, R.; Frens, W.; Linders, M.; Goetheer, E. Ember Pyrolysis Technology for Hydrogen and Carbon. Available online: https://www.aiche.nl/images/presentations/EMBER_Pyrolysis-technology-for-production-of-Hydrogen-and-carbon.pdf (accessed on 6 June 2024).
141. Giaconia, A.; Caputo, G.; Ienna, A.; Mazzei, D.; Schiavo, B.; Scialdone, O.; Galia, A. Biorefinery Process for Hydrothermal Liquefaction of Microalgae Powered by a Concentrating Solar Plant: A Conceptual Study. *Appl. Energy* **2017**, *208*, 1139–1149. [CrossRef]

142. Raikova, S.; Le, C.D.; Wagner, J.L.; Ting, V.P.; Chuck, C.J. Towards an Aviation Fuel Through the Hydrothermal Liquefaction of Algae. In *Biofuels for Aviation*; Elsevier: Amsterdam, The Netherlands, 2016; pp. 217–239. ISBN 9780128045688.
143. NIST. Thermophysical Properties of Fluid Systems. Available online: https://webbook.nist.gov/chemistry/fluid/ (accessed on 11 April 2025).
144. Tzanetis, K.F.; Posada, J.A.; Ramirez, A. Analysis of Biomass Hydrothermal Liquefaction and Biocrude-Oil Upgrading for Renewable Jet Fuel Production: The Impact of Reaction Conditions on Production Costs and GHG Emissions Performance. *Renew. Energy* **2017**, *113*, 1388–1398. [CrossRef]
145. Collares-Pereira, M.; Canavarro, D.; Guerreiro, L.L. *Advances in Concentrating Solar Thermal Research and Technology: 15.4 Advanced LFR and Molten Salts: A New Concept Plant*, 1st ed.; Blanco, M.J., Santigosa, L.R., Eds.; Woodhead Publishing: Amsterdam, The Netherlands; Boston, MA, USA; Heidelberg, Germany; London, UK; New York, NY, USA; Oxford, UK; Paris, France; San Diego, CA, USA; San Francisco, CA, USA; Singapore, 2017; ISBN 9780081005163.
146. Giaconia, A.; De Falco, M.; Caputo, G.; Grena, R.; Tarquini, P.; Marrelli, L. Solar Steam Reforming of Natural Gas for Hydrogen Production Using Molten Salt Heat Carriers. *AIChE J.* **2008**, *54*, 1932–1944. [CrossRef]
147. Giaconia, A.; Iaquaniello, G.; Caputo, G.; Morico, B.; Salladini, A.; Turchetti, L.; Monteleone, G.; Giannini, A.; Palo, E. Experimental Validation of a Pilot Membrane Reactor for Hydrogen Production by Solar Steam Reforming of Methane at Maximum 550 °C Using Molten Salts as Heat Transfer Fluid. *Int. J. Hydrogen Energy* **2020**, *45*, 33088–33101. [CrossRef]
148. Sanz-Bermejo, J.; Muñoz-Antón, J.; Gonzalez-Aguilar, J.; Romero, M. Optimal Integration of a Solid-Oxide Electrolyser Cell into a Direct Steam Generation Solar Tower Plant for Zero-Emission Hydrogen Production. *Appl. Energy* **2014**, *131*, 238–247. [CrossRef]
149. Monforti Ferrario, A.; Santoni, F.; Della Pietra, M.; Rossi, M.; Piacente, N.; Comodi, G.; Simonetti, L. A System Integration Analysis of a Molten Carbonate Electrolysis Cell as an Off-Gas Recovery System in a Steam-Reforming Process of an Oil Refinery. *Front. Energy Res.* **2021**, *9*, 655915. [CrossRef]
150. Frangini, S.; Della Pietra, M.; Della Seta, L.; Paoletti, C.; Pedro Pérez-Trujillo, J. Degradation of MCFC Materials in a 81 Cm2 Single Cell Operated Under Alternated Fuel Cell/Electrolysis Mode. *Front. Energy Res.* **2021**, *9*, 653531. [CrossRef]
151. Roeb, M.; Thomey, D.; de Oliveira, L.; Sattler, C.; Fleury, G.; Pra, F.; Tochon, P.; Brevet, A.; Roux, G.; Gruet, N.; et al. Sulphur Based Thermochemical Cycles: Development and Assessment of Key Components of the Process. *Int. J. Hydrogen Energy* **2013**, *38*, 6197–6204. [CrossRef]
152. Gorensek, M.B.; Corgnale, C.; Summers, W.A. Development of the Hybrid Sulfur Cycle for Use with Concentrated Solar Heat. I. Conceptual design. *Int. J. Hydrogen Energy* **2017**, *42*, 20939–20954. [CrossRef]
153. Norman, J.; Mysels, K.; Sharp, R.; Williamson, D. Studies of the Sulfur-Iodine Thermochemical Water-Splitting Cycle. *Int. J. Hydrogen Energy* **1982**, *7*, 545–556. [CrossRef]
154. Kalyva, A.E.; Vagia, E.C.; Konstandopoulos, A.G.; Srinivasa, A.R.; T-Raissi, A.; Muradov, N.; Kakosimos, K.E. Hybrid Photo-Thermal Sulfur-Ammonia Water Splitting Cycle: Thermodynamic Analysis of the Thermochemical Steps. *Int. J. Hydrogen Energy* **2017**, *42*, 9533–9544. [CrossRef]
155. Tizzoni, A.C.; Mansi, E.; Sau, S.; Spadoni, A.; Corsaro, N.; Lanchi, M.; Giorgi, G.; Turchetti, L.; Delise, T. Thermochemical Cycle Based on Solid Intermediates for Hydrogen Storage and On-Demand Production. *E3S Web Conf.* **2022**, *334*, 01006. [CrossRef]
156. Abanades, S. Metal Oxides Applied to Thermochemical Water-Splitting for Hydrogen Production Using Concentrated Solar Energy. *ChemEngineering* **2019**, *3*, 63. [CrossRef]
157. Padella, F.; Alvani, C.; La Barbera, A.; Ennas, G.; Liberatore, R.; Varsano, F. Mechanosynthesis and Process Characterization of Nanostructured Manganese Ferrite. *Mater. Chem. Phys.* **2005**, *90*, 172–177. [CrossRef]
158. Sakurai, M.; Bilgen, E.; Tsutsumi, A.; Yoshida, K. Solar UT-3 Thermochemical Cycle for Hydrogen Production. *Sol. Energy* **1996**, *57*, 51–58. [CrossRef]
159. Doctor, R.D.; Marshall, C.L.; Wade, D.C. *Hydrogen Cycle Employing Calcium-Bromine and Electrolysis*; Argonne National Laboratory: Argonne, IL, USA, 2002.
160. Naterer, G.F.; Suppiah, S.; Stolberg, L.; Lewis, M.; Wang, Z.; Rosen, M.A.; Dincer, I.; Gabriel, K.; Odukoya, A.; Secnik, E.; et al. Progress in Thermochemical Hydrogen Production with the Copper–Chlorine Cycle. *Int. J. Hydrogen Energy* **2015**, *40*, 6283–6295. [CrossRef]
161. Angeli, S.D.; Turchetti, L.; Monteleone, G.; Lemonidou, A.A. Catalyst Development for Steam Reforming of Methane and Model Biogas at Low Temperature. *Appl. Catal. B Environ.* **2016**, *181*, 34–46. [CrossRef]
162. Turchetti, L.; Murmura, M.A.; Monteleone, G.; Giaconia, A.; Lemonidou, A.A.; Angeli, S.D.; Palma, V.; Ruocco, C.; Annesini, M.C. Kinetic Assessment of Ni-Based Catalysts in Low-Temperature Methane/Biogas Steam Reforming. *Int. J. Hydrogen Energy* **2016**, *41*, 16865–16877. [CrossRef]

163. Integrating National Research Agendas on Solar Heat for Industrial Processes | INSHIP | Project | Fact Sheet | H2020 | CORDIS | European Commission. Available online: https://cordis.europa.eu/project/id/731287 (accessed on 6 June 2024).
164. Zhang, Y.; Liang, Y.; Li, S.; Yuan, Y.; Zhang, D.; Wu, Y.; Xie, H.; Brindhadevi, K.; Pugazhendhi, A.; Xia, C. A Review of Biomass Pyrolysis Gas: Forming Mechanisms, Influencing Parameters, and Product Application Upgrades. *Fuel* **2023**, *347*, 128461. [CrossRef]

Disclaimer/Publisher's Note: The statements, opinions and data contained in all publications are solely those of the individual author(s) and contributor(s) and not of MDPI and/or the editor(s). MDPI and/or the editor(s) disclaim responsibility for any injury to people or property resulting from any ideas, methods, instructions or products referred to in the content.